

What determines the strength and the slowdown rate of bars ?

E. Athanassoula

Observatoire de Marseille, 2 Place Le Verrier, F-13248 Marseille Cedex 4, France

Accepted . Received ;

ABSTRACT

Isolated barred galaxies evolve by redistributing their angular momentum, which, emitted by material in the inner disc at resonance with the bar, can be absorbed by resonant material in the outer disc, or in the halo. The amount of angular momentum that can be emitted/absorbed at a given resonance depends on the distribution function of the emitting/absorbing material. It thus depends not only on the amount of material on resonant orbits, but also on the velocity dispersion of that material. As it loses angular momentum, the bar becomes stronger and it also rotates slower. Thus the strength of the bar and the decrease of its pattern speed with time are set by the amount of angular momentum exchanged within the galaxy, which, in turn, is regulated by the mass distribution and the velocity dispersion of the material in the disc and spheroidal components. Correlations between the pattern speed of the bar, its strength and the angular momentum absorbed by the spheroid (halo plus bulge) argue strongly that it is the amount of angular momentum exchanged that determines the strength and the slowdown rate of the bar. The decrease of the bar pattern speed with time should not be used to set constraints on the halo-to-disc mass ratio, since it depends also on the velocity dispersion of the halo and disc material.

Key words: galaxies: structure – galaxies: kinematics and dynamics – barred galaxies – methods: numerical.

1 INTRODUCTION

Leafing through an atlas of galaxies (e.g. Sandage 1961, Sandage & Bedke 1988) or looking at images of barred galaxies on different web sites one sees that bars come in a variety of shapes and sizes. From the strong bars, like in NGC 1365, NGC 1300 and NGC 5383, to the small bars confined to the central parts, like in our own Galaxy, and to the ovals, like in NGC 1566, all possible lengths and strengths are covered. Several studies have been devoted to finding some systematic trends in their properties. Athanassoula & Martinet (1980) and Martin (1995) found a correlation between the length of the bar and the size of the bulge components, while Elmegreen & Elmegreen (1985) showed that there is a clear dependence of the bar length on the galaxy type, in the sense that early type disc galaxies have longer bars than late types. Similarly, Fourier analysis of the de-projected light distribution of barred galaxies, shows (Ohta 1996 and references therein) that early types have considerably higher values for their $m = 2, 4, 6$ and 8 Fourier components. These works, and several others, point to the fact that bars in early type disc galaxies are on average stronger than those in later types.

Bar pattern speeds are much more difficult to measure. Observational determinations are either indirect (e.g. from the location of rings, or from fits of gas flow models to velocity field data), or with the help of the Tremaine & Weinberg (1984b) method. The value of the pattern speed at a given time is a function of its initial value, as well as of its change during the evolution. The latter of course is not possible to determine observationally, until observations of far away galaxies become sufficiently detailed to allow it to be estimated.

So what determines the strength of a bar and the evolution of its pattern speed? In this paper I will use both analytical calculations and N -body simulations to argue that it is the angular momentum exchange between different parts of a galaxy. The role of the angular momentum exchange has already been discussed in many papers. First and foremost, the ground-breaking paper of Lynden-Bell & Kalnajs (1972, hereafter LBK), who argue that angular momentum exchange is the mechanism that generates spirals. Mark (1976) discussed wave amplification through processes that remove angular momentum from galactic discs, while Kormendy (1979) proposed that the angular momentum exchange between the bar and the spheroid could drive secu-

lar evolution. Sellwood (1980) was the first to measure in an N -body simulation the angular momentum exchange between the disc and the halo component. Tagger et al. (1987) and Sygnet et al. (1988) showed that mode coupling allows a galaxy to transfer angular momentum over a larger radial interval than what a single mode would have allowed. The link between angular momentum and bar slowdown has been made in many papers (Tremaine & Weinberg 1984a; Weinberg 1985; Little & Carlberg 1991a, 1991b; Hernquist & Weinberg 1992, Athanassoula 1996; Debattista & Sellwood 1998, 2000; Valenzuela & Klypin 2002), out of which some calculated, or at least emphasized, the role of resonant stars (Tremaine & Weinberg 1984a, Weinberg 1985, Little & Carlberg 1991a, Hernquist & Weinberg 1992). The link between the angular momentum exchange and the bar strength has been addressed only recently (Athanassoula 2002a, hereafter A02). Although all these papers show a general qualitative agreement, in the sense that bars grow stronger and slow down as they evolve, quantitatively they disagree. Not much effort has been put in understanding the reason for these differences, which were even some times attributed to inadequacies of either the codes or the models.

In this paper, I will argue that it is the angular momentum exchange within the galaxy that determines the bar growth and its slowdown. I will seek what influences the angular momentum exchange and therefore the bar strength and slowdown rate. In section 2, I will present some, mainly linear, 3D theoretical work, which I will apply to the disc and to the spheroidal (halo and bulge) components separately. This will allow me to determine which parts of the galaxy gain and which parts lose angular momentum and also to get some insight about the quantities that can influence the amount exchanged. In section 3, I will discuss resonances and their link to the disc orbital structure. Section 4 introduces the simulations and section 5 discusses the angular momentum exchange. Sections 6, 7, and 8 discuss the effect of the disc-to-halo mass ratio and of the velocity dispersions. Section 9 presents correlations, based on the results of a very large number of simulations, that establish the link between the angular momentum exchange and the bar strength and pattern speed. Finally, in section 10, I summarise and present a general discussion, including the applicability of the simulation results to real galaxies and the conclusions that can be reached.

2 ANALYTICAL CALCULATIONS

Using linear theory, it is possible to follow the angular momentum redistribution. For this I will follow the method already outlined in several papers (LBK, Kato 1971, Weinberg & Tremaine 1984a, Weinberg 1985 etc.). I will thus use Hamilton-Jacobi variables (J_i, w_i) , where J_i are the canonical momenta, w_i are the angles and $i = 1, 2, 3$. The equations of motion of a given particle are then

$$\dot{J}_i = -\frac{\partial H_0}{\partial w_i} = 0, \quad \dot{w}_i = \frac{\partial H_0}{\partial J_i} \equiv \Omega_i, \quad (1)$$

where Ω_i are the frequencies and H_0 is the unperturbed Hamiltonian. The potential Ψ can be written as a sum of an axisymmetric component Ψ_0 and a perturbation, i.e.

$$\Psi = \Psi_0 + \psi e^{i\omega t}, \quad (2)$$

where ω is the wave frequency. Its real part ω_R gives the pattern speed, $\omega_R = \Omega_p/m$, and its imaginary part, ω_I , gives the growth rate. Since the angle variables are periodic in phase space with period 2π , the potential perturbation can be expanded in a Fourier series.

$$\psi(J_i, w_i) = \frac{1}{8\pi^3} \sum_{l,m,n} \psi_{lmn}(J_i) e^{i(lw_1 + mw_2 + nw_3)}. \quad (3)$$

The coefficients ψ_{lmn} are given by

$$\begin{aligned} \psi_{lmn}(J_i) = \int_0^{2\pi} \int_0^{2\pi} \int_0^{2\pi} dw_1 dw_2 dw_3 \\ \times \psi(J_i, w_i) e^{-i(lw_1 + mw_2 + nw_3)}. \end{aligned} \quad (4)$$

Similar equations can be written for the perturbation of the distribution function and of the density.

LBK calculated the change of an orbit due to the potential perturbation. To first order one can calculate the forces along the unperturbed orbit. In this case, the changes in the actions $\Delta_1 J_i$ are periodic in the angle variables w_i . Therefore, for particles distributed uniformly in w_i , the average gain in angular momentum^{*} (obtained by integrating over w_i) is zero, i.e. particles can neither give nor take angular momentum. Thus the change is of second order and has to be obtained by calculating the forces along the perturbed orbit. To obtain the total change in angular momentum one has to integrate over the unperturbed distribution function F . Following LBK, I get

$$\begin{aligned} \dot{L}_z = \frac{1}{8\pi^2} \omega_I e^{-2\omega_I t} \int \int \int dJ_1 dJ_2 dJ_3 \\ \times \sum_{l,m,n} \frac{m \left(l \frac{\partial F}{\partial J_1} + m \frac{\partial F}{\partial J_2} + n \frac{\partial F}{\partial J_3} \right)}{|\Omega_1 + m\Omega_2 + n\Omega_3 + \omega|^2} |\psi_{lmn}|^2, \end{aligned} \quad (5)$$

where L_z is the z component of the angular momentum, and the integration is carried over all the available action space. If $\omega_I = 0$, then the integral on the right side is non-zero only at the resonances, i.e. where

$$l\Omega_1 + m\Omega_2 + n\Omega_3 = -\omega_R = m\Omega_p \quad (6)$$

On the other hand, in the case of a non-zero ω_I , this integral is non-zero even away from resonances, i.e. angular momentum can be emitted or absorbed even away from resonances. This contribution, however, will be small if the value of ω_I is not large. For $\omega_I \rightarrow 0$ one can write

$$\begin{aligned} \dot{L}_z = -\frac{1}{8\pi} \int \int \int dJ_1 dJ_2 dJ_3 \\ \times \sum_{l,m,n} m \left(l \frac{\partial F}{\partial J_1} + m \frac{\partial F}{\partial J_2} + n \frac{\partial F}{\partial J_3} \right) \\ \times |\psi_{lmn}|^2 \delta(l\Omega_1 + m\Omega_2 + n\Omega_3 + \omega). \end{aligned} \quad (7)$$

^{*} in the following I will often loosely refer to the z component of the angular momentum as the angular momentum.

This equation is particularly useful if one wishes to find which resonances emit angular momentum and which absorb it, and will be discussed later, separately for the disc and spheroidal components. Integrating eq. (5) over time I can find the total change of angular momentum

$$\Delta L_z = -\frac{1}{16\pi^2} e^{-2\omega_I t} \int \int \int dJ_1 dJ_2 dJ_3 \times \sum_{l,m,n} \times \frac{m \left(l \frac{\partial F}{\partial J_1} + m \frac{\partial F}{\partial J_2} + n \frac{\partial F}{\partial J_3} \right)}{|l\Omega_1 + m\Omega_2 + n\Omega_3 + \omega|^2} |\psi_{lmn}|^2. \quad (8)$$

Thus linear theory predicts a direct relationship between the perturbing potential ψ and the change of angular momentum ΔL_z . In the simple case of an external forcing due to a companion (e.g. Berentzen, Athanassoula, Heller et al. 2003) or to a rigid bar (e.g. Weinberg 1985, Hernquist and Weinberg 1992) on a given target disc, this equation will imply a correlation between the change in angular momentum and the amplitude of the external forcing. In the more general case, however, of the self consistent evolution of different disc/halo configurations, as those considered in the present paper, the relation between the bar strength and the change of angular momentum, although straightforward, is not an exact correlation, since different cases will have different distribution functions and different forms of perturbation potentials.

The above equations make no predictions about the pattern speed. This, in the case of modes, is set by the mode conditions, and, in cases with external forcing, by the pattern speed of the forcing. Thus, to find the relation between the exchange of angular momentum and the pattern speed, one should apply nonlinear theory. For the bar component, considered as a solid body, I can write

$$L_{z,B} = I \Omega_p, \quad (9)$$

where $L_{z,B}$ is the bar angular momentum, Ω_p is the pattern speed of the bar and I is its moment of inertia. If most of the angular momentum lost by the bar was taken by the spheroid, then I can assume that the angular momentum of the outer part of the disc does not change with the evolution and thus I can, for this case, write $L_{D,inner} - I \Omega_p = L_S$, where $L_{D,inner}$ is the angular momentum of the inner disc initially and L_S is the angular momentum taken by the spheroid, which, if the spheroid was initially non-rotating, is just the total angular momentum of the halo and bulge components at the time under consideration. Thus in such a case I would expect, at any given time, a simple linear relation between the bar pattern speed and the angular momentum taken by the spheroid.

The evolution of the bar angular momentum can be given as

$$\frac{dL_{z,B}}{dt} = \frac{d(I \Omega_p)}{dt}. \quad (10)$$

The change of angular momentum will thus depend not only on the change of Ω_p , but also on the change of the moment of inertia. One thus expects the change of the angular momentum to be directly proportional to the change of the bar pattern speed only if the momentum of inertia of the bar does not change, i.e. if the bar is rigid (as e.g. for Weinberg

1985, or Hernquist and Weinberg 1992). This is not true in a general case where the bar evolves self-consistently, since both the bar pattern speed and its moment of inertia change with time.

Eq. (8) can be somewhat simplified if one considers the disc and halo components separately.

2.1 Disc component

For the disc component one can neglect the z dimension and obtain eq. (29) of LBK. In the epicyclic approximation

$$\Omega_1 = \kappa, \quad \Omega_2 = \Omega, \quad (11)$$

$$J_1 = \frac{1}{2} \kappa a^2, \quad J_2 = L_z, \quad (12)$$

where Ω and κ are the angular and epicyclic frequencies respectively and a is the amplitude of the epicyclic oscillation. Furthermore, in this approximation

$$\left| \frac{\partial F}{\partial J_1} \right| \gg \left| \frac{\partial F}{\partial J_2} \right|, \quad (13)$$

so that for l different from 0 one may retain in eq. (7) only the first term of the quantity in parenthesis, i.e. $l \frac{\partial F}{\partial J_1}$. Since $\frac{\partial F}{\partial J_1} < 0$ for any sensible distribution function, the sign of the product lm will determine whether angular momentum is gained or lost at the resonance defined by those l and m . For $l = 0$ the first term vanishes, so that \dot{L}_z will always be positive. In general, however, the contribution of this resonance will in general be absolutely smaller than the corresponding terms for l different than zero, because of inequality (13).

By recasting eq. (7), LBK showed that the perturbation has negative energy and angular momentum within corotation (see also Kalnajs 1971). This means that, if energy or angular momentum is given to it, it will be damped, while if it is taken from it it will be excited.

If I use the standard form of the disc distribution function

$$F_0(J_1, J_2) = \frac{1}{(2\pi)^2 < J_1 >} \Sigma_d(J_2) e^{-J_1 / < J_1 >}, \quad (14)$$

I see that $\frac{\partial F}{\partial J_1}$ is equal to $-F / < J_1 >$, or, using eq. (12), inversely proportional to the root mean square of the epicyclic amplitude. This means that, for the same perturbing potential, a given resonance will absorb, or emit, considerably more angular momentum if its stars are cold, rather than hot.

2.2 Bulge and halo components

Like the particles in the disc component, for a steady forcing, particles in the bulge or the halo can emit/absorb angular momentum only if they are at resonance. In the case of a growing or decaying perturbation, all particles can emit/absorb angular momentum, but the amount is small unless the perturbation is strongly growing or decaying. A02a showed that the halo component can have a considerable amount of resonant and near-resonant orbits, because of its response to the bar. The distribution functions of the halo and bulge should be less sharply peaked than that of the disc because these components are hotter. Therefore one expects the amount of angular momentum emitted or absorbed

per unit mass at resonance to be smaller for the halo than for the disc component. But, since the halo is heavier than the disc, its contribution to the total angular momentum exchange could be considerable.

The epicyclic approximation can not be applied to the spheroids. Eq. (7) can, nevertheless, be simplified by assuming that the distribution function depends only on the energy. Using eq. (1), I get

$$l \frac{\partial F}{\partial J_1} + m \frac{\partial F}{\partial J_2} + n \frac{\partial F}{\partial J_3} = \frac{\partial F}{\partial E} (l\Omega_1 + m\Omega_2 + n\Omega_3). \quad (15)$$

Then, using the resonant condition (6), eq. (7) can be written

$$\begin{aligned} \dot{L}_z = & -\frac{1}{8\pi} \int \int \int dJ_1 dJ_2 dJ_3 \\ & \times \sum_{l,m,n} m^2 \Omega_p \left(\frac{\partial F}{\partial E} \right) |\psi_{lmn}|^2 \delta(l\Omega_1 + m\Omega_2 + n\Omega_3 + \omega). \end{aligned} \quad (16)$$

Note that all terms in the summation have the same sign, independent of the values of l, m and n . In the physically reasonable case where the distribution function is a decreasing function of the energy, I get $\dot{L}_z > 0$, which means that, as long as the distribution function depends only on the energy, *all* halo or bulge resonances gain angular momentum.

Similarly eq. (8) simplifies to

$$\begin{aligned} \Delta L_z = & -\frac{1}{16\pi^2} e^{-2\omega t} \int \int \int dJ_1 dJ_2 dJ_3 \\ & \times \sum_{l,m,n} \frac{m^2 \Omega_p \frac{\partial F}{\partial E} |\psi_{lmn}|^2}{|l\Omega_1 + m\Omega_2 + n\Omega_3 + \omega|^2}. \end{aligned} \quad (17)$$

This gives the total angular momentum that will be gained by the spheroid. Since $\frac{\partial F}{\partial E}$ is absolutely larger for colder distributions, these will be able to absorb more angular momentum than hotter ones.

3 RESONANCES AND ORBITAL STRUCTURE IN THE DISC COMPONENT

The previous section underlined the importance of resonances in the evolution of the galaxy. Here I will discuss the orbital structure at resonances, focusing on the parts that will be essential in understanding the simulation results described in the following sections.

3.1 Resonant orbits

The planar resonances occur for $n = 0$. With this restriction and using eqs. (11), the resonant condition (6) can be simply written as

$$l\kappa + m\Omega = -\omega_R = m\Omega_p \quad (18)$$

For $l = -1$ and $m = 2$ one has the inner Lindblad resonance (hereafter ILR), while for $l = 1$ and $m = 2$ one has the outer Lindblad resonance (hereafter OLR). For the former $lm < 0$, so that disc particles at this resonance will lose angular momentum, the opposite being true for the OLR. The

same will be true for larger values of m , so that particles at the $(l, m) = (-1, 3), (-1, 4), (-1, 5)$ etc. resonances will lose angular momentum and particles at the $(l, m) = (1, 3), (1, 4), (1, 5)$ etc. resonances will gain it. There are also resonances for $|l| > 1$, but these are higher order and therefore should be of lesser dynamical importance. For $l = 0$ one has the corotation radius (hereafter CR), at which the angular frequency of the particle is equal to the pattern frequency.

Resonant orbits are easy to visualise. For example orbits at the ILR will, in the frame of reference of the bar, close after one revolution around the center and two radial oscillations. Similarly, orbits at the $(-1, 4)$ resonance will close after one revolution and four radial oscillations etc. Orbits at the higher order resonances, where $|l| > 1$, will close after more than one revolution.

Several papers have focused on the study of periodic orbits in barred galaxy potentials (see Contopoulos & Grosbøl 1989, for a review). They discuss in detail the properties of the x_1 and the x_1 -related orbits, which are the backbone of all orbital structure (Athanassoula, Bienayme, Martinet et al. 1983, Skokos, Patsis & Athanassoula 2002). The x_1 are periodic orbits that close after one revolution and two radial oscillations. *Therefore all x_1 orbits are $l = -1$ and $m = 2$ resonant orbits, i.e. ILR resonant orbits.* This simple fact has not been generally noted so far, and this has led to a number of misunderstandings, one of which I will discuss below, since it is linked with the very definition of the ILR. The x_1 -related orbits are 3D periodic orbits whose families bifurcate from the vertical instabilities of the x_1 family. Their properties have been described by Skokos et al. (2002). At higher energies and farther from the center one finds the $(1, 3), (1, 4), (1, 5)$ etc. families of periodic orbits. Their orbits close after one revolution and 3, 4, 5, ... oscillations, respectively. Members of these families are therefore also resonant orbits with $l = -1$ and $m = 3, 4, 5$ etc.. As m increases we approach corotation, but families with high m values are crowded together on the characteristic diagram (e.g. fig. 2 of Athanassoula 1992) and have less extended stable parts. A similar sequence can be found outside corotation for $l = 1$, starting with large m and moving outwards to the OLR as m decreases. Periodic orbits of both the outer and the inner sequence of families have been calculated for many barred potentials (see e.g. Contopoulos & Grosbøl 1989 for a review). Such orbital studies have also used surfaces of section to show that stable members of all these families can trap around them other orbits, which, in orbital structure studies, are usually referred to as regular or trapped orbits. They are in fact near-resonant orbits and can be thought of as a superposition of a periodic/resonant orbit and an oscillation around it. It is therefore possible to use all the results on the structure and stability of periodic orbits obtained in the extensive literature on the subject to the study of resonances and vice-versa. Unfortunately the terminology in these two fields is not always in agreement. A clear case of disagreement concerns the very definition of the ILR and its orbits, and stems from the fact that the frequencies Ω and κ of a single particle are equal to those of the galaxy at that radius only if the galaxy is near-axisymmetric and cold.

3.2 Definition of the ILR

Let us consider an axisymmetric galaxy with a non-axisymmetric small perturbation of pattern speed Ω_p . According to the standard linear definition, an ILR occurs if and where

$$\Omega - \kappa/2 = \Omega_p. \quad (19)$$

This may happen at one, two or no radii, which are called the ILR radii, and one correspondingly says the galaxy has one, two or no ILRs. Of course this definition is valid only for galaxies with non-axisymmetric perturbations of very low amplitude (e.g. Binney and Tremaine 1987). It can not be applied directly to strongly non-axisymmetric galaxies or models, since for such cases the potential and forces are a function of the angle as well as the radius, and thus Ω and κ can not be strictly defined and used as in the linear case. It is thus necessary to consider some extension of the linear definition. More than one is possible, and at least three have been so far proposed, which may in some cases contradict each other.

One way of extending the linear definition is by noting that the angular and epicyclic frequencies are the natural frequencies of the orbits in a given potential. Then the linear definition of the ILR is extended to eq. (18). Strictly speaking, this is the definition of a resonant orbit, not the definition of the existence of the resonance or of its radius. But one can extend it to say that a galaxy has an ILR resonance if it has ILR resonant orbits.

A different extension was adopted in orbital structure studies. In the axisymmetric – or near-axisymmetric – cases the various (l, m) families bifurcate from the x_1 at the corresponding resonances. This can be extended to the strongly nonlinear and non-axisymmetric cases by saying that resonances occur where there are gaps or bifurcations introducing new (l, m) families. In particular, in the axisymmetric case the families of $l = -1, m = 2$ orbits are bifurcated at the $(-1, 2)$ resonance(s). These families are called x_2 and x_3 and their orbits are oriented perpendicular to the bar. As the amplitude of the perturbation increases the bifurcations are substituted by gaps, but one can still say that an ILR resonance exists if and only if these x_2 and x_3 families exist (e.g. van Albada & Sanders 1982, Athanassoula 1992).

Finally in observational work, and often in the analysis of N -body simulations, the linear axisymmetric definition is extended very simply by defining for a given quantity, e.g. the mass, its axisymmetric equivalent, simply by averaging this quantity over the azimuthal angle. Thus the linear definition can be applied to strongly nonlinear and non-axisymmetric cases (e.g. Sanders & Tubbs 1980, Reynaud & Downes 1997).

Each of these extensions and corresponding definitions is reasonable and useful within its own context. They are, however, not fully compatible, and, in many cases, can lead to contradictions. For example with the first extension all barred galaxies have ILRs, since all have x_1 orbits, i.e. $l = -1, m = 2$ resonant orbits, and the resonant region is very broad, comparable to the bar size. The same barred galaxies, however, may, by the orbital structure definition, not have ILRs, if their potentials do not allow x_2 and x_3 families. Similarly Athanassoula (1992) showed a few examples where the orbital structure definition and the observational

definition are in contradiction (although in general there is agreement). It is beyond the scope of this paper to propose a solution to this nomenclature problem. I, nevertheless, want to underline it here, since it has often led to misunderstandings.

3.3 Orbits and bar angular momentum

Viewing the bar as an ensemble of orbits allows considerable insight. It shows that the bar has several, dynamically connected, ways of losing angular momentum. First, by trapping particles which were on quasi-circular orbit outside the bar, into elongated orbits in its outer parts. This way angular momentum is lost from the disc inner parts, while the bar will become longer, i.e. stronger. A second alternative is if part, or all, of the orbits trapped in the bar become more elongated. This way the bar loses angular momentum, while becoming thinner, i.e. stronger. Finally the bar can slow down its figure rotation, i.e. decrease its pattern speed, and again lose angular momentum. In fact these three possibilities should be linked. For example if a bar becomes longer, then it might have also to slow down in order to push its CR further out and thus make space for the newly trapped orbits in its outer parts (which must necessarily lie within CR). In section 9 I will also show that there is a general anti-correlation between the strength and the pattern speed of a bar. This shows that bars use more than one of the three alternatives at their disposal. Analytical calculations, however, are not capable of determining the extent to which each of the three alternatives will be used in a specific case.

The linear theory described in the first part of section 2 clearly predicts that more angular momentum can be emitted or absorbed at a given resonance if there are more absorbers/emitters and/or if they are colder. The change of the pattern speed with time enters only via the nonlinear equations (9) and (10), which relate the angular momentum of the bar with its strength and pattern speed. The change of pattern speed effects strongly the equilibrium between emitters and absorbers, since, to a first approximation, the two are divided by the CR. Since I here consider isolated galaxies, the total amount of angular momentum emitted at any time should be equal to the total amount absorbed. For lower values of the pattern speed corotation will be further out, so that there will be more particles trapped in the inner, $(-1, m)$, resonances which emit angular momentum. On the other hand, the resonances which absorb angular momentum will also be further out, both for the disc and the halo, and thus in regions of lower density, where less material can be marshaled into absorbing angular momentum. Thus lowering the pattern speed favours emitters and disfavors absorbers. There should thus be, for every case, an optimum radius dividing emitters from absorbers, for which emission will balance absorption. This optimum radius is linked to corotation and therefore to the pattern speed.

Pushed further, this line of thought allows us to predict which configurations will favour faster pattern speed and which slower ones. Indeed, in cases where the halo can not absorb much angular momentum – either because it has low density in the relevant regions, or because it is very hot – the role of the outer disc is important. Thus CR should not be too far out, so as to leave sufficient space for disc absorbers. The opposite can be the case for models, or galaxies, where

the haloes can absorb considerable amounts of angular momentum. In principle, and provided the halo is sufficiently receptive, CR could be located in the outermost parts of the disc.

4 SIMULATIONS AND NUMERICAL MISCELANEA

N -body simulations are a much easier test bed of the above theoretical predictions than real galaxies, since they allow us to ‘observe’ the halo component and also to ‘observe’ time evolution. In the remaining sections I will use them for this purpose.

The galaxies I model numerically consist initially of a disc, a halo, and sometimes a bulge component. The density distribution in the disc is given by

$$\rho_d(R, z) = \frac{M_d}{4\pi R_d^2 z_0} \exp(-R/R_d) \operatorname{sech}^2(z/z_0), \quad (20)$$

that in the bulge by

$$\rho_b(r) = \frac{M_b}{2\pi a^2} \frac{1}{r(1+r/a)^3}, \quad (21)$$

and that in the halo by

$$\rho_h(r) = \frac{M_h}{2\pi^{3/2}} \frac{\alpha}{r_c} \frac{\exp(-r^2/r_c^2)}{r^2 + \gamma^2}. \quad (22)$$

In the above r is the radius, R is the cylindrical radius, M_d , M_b and M_h are the masses of the disc, bulge and halo respectively, R_d is the disc radial scale length, z_0 is the disc vertical scale thickness, a is the bulge scale length, and γ and r_c are halo scale lengths. The former can be considered as a core radius, and will hereafter be loosely referred to as such. The parameter α in the halo density equation is a normalisation constant defined by

$$\alpha = [1 - \sqrt{\pi} q \exp(q^2) (1 - \operatorname{erf}(q))]^{-1}, \quad (23)$$

where $q = \gamma/r_c$ (Hernquist 1993). The halo velocity distribution is isotropic. In building the initial conditions I loosely followed Hernquist (1993) and Athanassoula & Misiriotis (2002, hereafter AM02). In some cases, as e.g. those described in section 8, I need a considerably more extended halo. I then use for the density the sum of two densities as in (22), making sure that the two put together give a reasonable total halo. When describing such cases, I will use the subscript 1 for all quantities referring to the inner halo component and 2 for those of the outer halo. The functional forms for the two are identical.

The results presented in this paper are based on 160 simulations. These include mainly (roughly 80%) simulations made with the Marseille Grape-5 computers (for a description of Grape-5 boards and their performance see Kawai et al. 2000), using a tree-code specifically adapted to this hardware, while roughly 20% of the simulations were run with W. Dehnen’s treecode on PC workstations (Dehnen 2000, 2002). The results from the two codes agree well, as I could show by running a few simulations with both codes. In most of the simulations all particles had the same mass, but in 10 simulations I used particles of different masses. To make sure that this did not introduce any bias I first calculated the pericenter of each particle orbit in the initial configuration and then sorted the particles as a function

of this quantity. The largest masses were then attributed to particles with the largest pericenters, thus ensuring that these particles will never reach too near the center. Since the halo density distribution does not change much with time (AM02), these particles will not visit the inner regions even after the model has evolved. Using the pericenter in order to attribute the particle masses is much safer than using the distance of the particle from the center at $t = 0$, since many particles will be near their apocenters at this time. Such particles, following their orbits, may visit at later times the inner parts where the disc with the lighter particles resides. This may introduce a bias in the evolution.

In previous papers (e.g. AM02, A02 etc.) I called MH (for Massive Halo) simulations with small cores, i.e. small γ values, for which the halo dominates in the inner parts. I called MD (for Massive Disc) simulations with large cores (γ values), where the disc dominates in the inner parts. This will carry over in this paper, but since I will here discuss a very large number of such simulations, I will rather use the names MH-type and MD-type.

Listing the initial condition parameters for all 160 simulations would be too lengthy, so I include in Table 1 only those runs which will be discussed in more detail in this paper. From left to right the columns give the name of the run, the mass and scale length of the exponential disc, the value of Q at $R = 0.1$ and a symbol denoting whether Q is a function of radius (v), or not (c). Then follow the three parameters describing the halo, namely its mass and its two scale lengths. The next three columns give the same parameters for the second halo, whenever this exists, and the last column gives the truncation radius of the mass distribution. This table lists all masses taken out to infinity.

A reasonable calibration, allowing to convert computer units to astronomical ones, has been given by AM02. They have taken the unit of mass equal to $5 \times 10^{10} M_\odot$, the unit of length equal to 3.5 kpc and $G = 1$. This gives that the unit of velocity is 248 km/sec and the unit of time is 1.4×10^7 yrs. This calibration is not unique and other ones can be equally good, depending on the application. I will thus present here all results in computer units and let the reader do the conversion according to his/her needs. Care, however, is necessary if one wants to compare the results of the simulations quantitatively to observations, since the length scale of the disc evolves with time (Valenzuela & Klypin 2002). Thus, when comparing with observations, one should not compare the observed disc scale length with the disc scale length of the initial conditions. One should instead fix a time at which the simulations should be compared to the observations, well after the bar has grown, and then compare the scale length obtained from that time to the observed one. Although this warning is in fact just common sense, its neglect has led to a number of errors and misunderstandings.

In most simulations the total number of particles used was between 1 and 2 million and I used a softening of 0.0625, or, in some cases, 0.03125. I repeated a few simulations with double and/or half the number of particles to make sure that the number used was sufficient. I further assessed the numerical robustness of my results by repeating some of the simulations with half and/or double the softening length and/or time step. Finally the comparison of the results obtained with the Grape-5 treecode, and those obtained with W. Dehnen’s treecode argue strongly for the reliability of

Table 1. Initial conditions for some of the models

model	M_d	R_d	z_0	Q	$Q(r)$	M_b	a	M_{h1}	γ_1	r_{c1}	M_{h2}	γ_2	r_{c2}	r_{trunc}
MB0	1.	1.	0.1	0.9	c	0.6	0.4	5.	6.	10.	0	–	–	15
MQ1	1.	1.	0.2	0.1	c	0	–	5.	0.5	10.	0	–	–	15
MQ2	1.	1.	0.2	0.9	c	0	–	5.	0.5	10.	0	–	–	15
MQ3	1.	1.	0.2	1.2	c	0	–	5.	0.5	10.	0	–	–	15
MQ4	1.	1.	0.2	1.4	c	0	–	5.	0.5	10.	0	–	–	15
MQ5	1.	1.	0.2	1.6	c	0	–	5.	0.5	10.	0	–	–	15
MQ6	1.	1.	0.2	1.8	c	0	–	5.	0.5	10.	0	–	–	15
MQ7	1.	1.	0.2	2.0	c	0	–	5.	0.5	10.	0	–	–	15
MQ8	1.	1.	0.2	2.2	c	0	–	5.	0.5	10.	0	–	–	15
MQV1	1.	1.	0.2	0.9	v	0	–	5.	0.5	10.	0	–	–	15
MQV2	1.	1.	0.2	1.	v	0	–	5.	5.	10.	0	–	–	15
MDQ	1.	1.	0.2	1.	c	0	–	5.	5.	10.	0	–	–	15
M γ 1	1.	1.	0.2	1.2	c	0	–	5.	0.01	10.	0	–	–	15
M γ 2	1.	1.	0.2	1.2	c	0	–	5.	0.1	10.	0	–	–	15
M γ 3	1.	1.	0.2	1.2	c	0	–	5.	0.5	10.	0	–	–	15
M γ 4	1.	1.	0.2	1.2	c	0	–	5.	1.	10.	0	–	–	15
M γ 5	1.	1.	0.2	1.2	c	0	–	5.	2.5	10.	0	–	–	15
M γ 6	1.	1.	0.2	1.2	c	0	–	5.	4.	10.	0	–	–	15
M γ 7	1.	1.	0.2	1.2	c	0	–	5.	5.	10.	0	–	–	15
MHH1	1.	1.	0.2	0.9	c	0	–	5.	0.5	10.	10	10	15	25
MHH2	1.	1.	0.2	0.9	c	0	–	5.	0.5	10.	10	4	15	25
MHH3	1.	1.	0.2	0.9	c	0	–	5.	0.5	10.	20	10	15	25
MH1	1.	1.	0.2	1.2	c	0	–	2.	0.5	10.	0	–	–	15
MH2	1.	1.	0.2	1.2	c	0	–	1.	0.5	10.	0	–	–	15
MH3	1.	1.	0.2	0.9	c	0	–	6.25	0.5	10.	0	–	–	15
MH4	1.	1.	0.2	0.9	c	0	–	8.333	0.5	10.	0	–	–	15

the results. I made an ultimate, very strong test, by running one case with a direct summation code. Since this is the code that has the least numerical assumptions, the very good agreement between those results and those obtained with a Grape-5 treecode argues strongly for the reliability of the code.

In simulations like those presented here one has to be particularly careful that numerical problems do not stop the resonant particles from gaining/losing angular momentum. This would be the case if, for example, the softening was too small for the adopted number of particles, in which case the simulation would be noisy. Encounters would be important and would knock particles off their resonant trajectories and thus artificially limit the angular momentum that could be emitted or absorbed by the resonances. Therefore, a simulation with a smaller softening is not necessarily better than one with a bigger softening. It can in some cases be worse, if the number of particles in the disc and/or halo is not sufficiently high. The most difficult cases to check are those with individual softening and/or individual mass. Indeed, it suffices that the simulation is noise dominated in one region for the resonant orbits traversing that region to have a high probability of being artificially scattered.

In this paper I discuss the bar strength and its evolution, and compare the strength of bars in different simulations. Although the notion of bar strength is clear to everyone, and it is very often easy, when comparing two bars, to say which one is strongest, a precise definition is not trivial. Several possibilities have been put forward so far, ranging from the bar axial ratio, to some function of the tangential forcing. Here I wish to stay as near as possible to the theoretical work presented in section 2, and so I will use the $m =$

2 component of the mass or density distribution in the disc. This has the added advantage that it can also be applied to observations, thus permitting a direct comparison between theory, N -body simulations and observations. Thus, following the notation of AM02, I quantify the bar strength with the help of the Fourier components of the face-on density or mass distribution. For a given m I will use the relative Fourier amplitudes $\sqrt{A_m^2 + B_m^2}/A_0$, where

$$A_m(r) = \frac{1}{\pi} \int_0^{2\pi} \Sigma(r, \theta) \cos(m\theta) d\theta, \quad m = 0, 1, 2, \dots \quad (24)$$

$$B_m(r) = \frac{1}{\pi} \int_0^{2\pi} \Sigma(r, \theta) \sin(m\theta) d\theta, \quad m = 1, 2, \dots \quad (25)$$

and $\Sigma(r, \theta)$ is the projected surface density, or mass. The above equations define the Fourier components, which are a function of the radius. To measure the strength of the bar, however, I want a single quantity, and not a function of radius. For this I take

$$S_B = \frac{\int_0^{R_{max}} \sqrt{A_m^2 + B_m^2} r dr}{\int_0^{R_{max}} A_0 r dr}, \quad (26)$$

It is easy to extend this definition to include higher m values, but I have refrained from doing so in order to stay as near the linear theory as possible. I have also used an alternative definition, without the r factor in the integrands of the numerator and denominator. The results are qualitatively similar.

In section 5 I will discuss resonant stars and the angular momentum they lose or gain. The procedure involved is a straightforward extension of that outlined in A02. I first

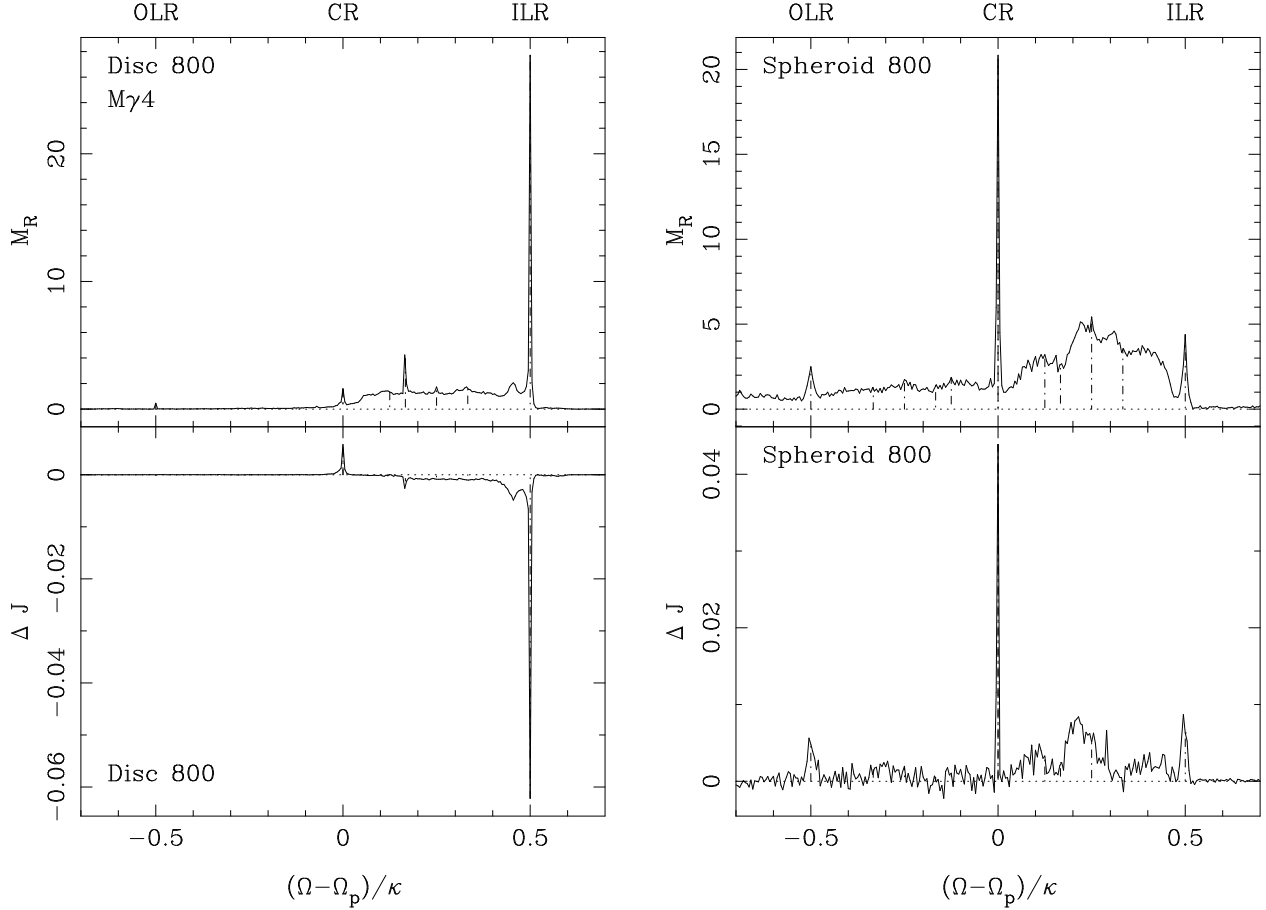


Figure 1. The upper panels give, for time $t = 800$, the mass per unit frequency ratio, M_R , as a function of that ratio. The lower panels give ΔJ , the angular momentum gained or lost by the particles between times 800 and 500, plotted as a function of their frequency ratio $(\Omega - \Omega_p)/\kappa$, calculated at time $t = 800$. The left panels correspond to the disc component and the right ones to the spheroid. The component and the time are written in the upper left corner of each panel. The vertical dot-dashed lines give the positions of the main resonances.

freeze the potential at a given time in the simulation, allowing only the bar to rotate rigidly with a pattern speed equal to that in the simulation. I then calculate in this potential the orbits of 100 000 particles taken at random from the disc population, and 100 000 particles taken at random from the spheroid population. For each orbit, I calculate the principal frequencies Ω and κ using spectral analysis. Since the angular frequency proved more difficult to calculate reliably, I supplemented the spectral analysis with other, more straightforward methods, based on following the angle as a function of time. I then binned the particles in bins of width $\Delta(\frac{\Omega - \Omega_p}{\kappa}) = 0.005$, calculated the mass within each bin, and, dividing the mass in the bin by its width, I obtained the mass per unit frequency of the bin, M_R . This is somewhat different from what I did in A02, where I used number, rather than mass, densities. Number and mass densities are equivalent for A02, since in the simulations discussed there all particles have the same mass. Since now in a few of my simulations this is not the case, it was necessary to introduce this modification. I also calculated the mean angular momentum of the orbit, where the time average was taken over 40 bar rotations of the frozen potential. One can thus associate at any given time a frequency ratio $(\Omega - \Omega_p)/\kappa$ and an angular momentum. The error estimates are as discussed in

A02, and the orbits for which the estimates of the frequencies were not considered sufficiently reliable were not used in any further analysis. This was of the order of, or less than, 15%.

5 ANGULAR MOMENTUM EXCHANGE

I will use the N -body simulations introduced above to test whether the analytical results developed in section 2 can still be applied to cases as non-axisymmetric and as non-linear as strongly barred galaxies. The linear theory predicts that angular momentum is gained by the resonant particles in the halo, the bulge and the outer disc and is lost by the resonant particles in the bar. Since the bar is a strongly non-linear feature, the agreement should be, at best, qualitative, rather than quantitative.

In A02 I showed that there are indeed a lot of resonant and near-resonant particles, both in the disc and the halo. It is possible to extend this work to test for the angular momentum lost or gained at various resonances. The results, for a run listed in Table 1 as M74, are plotted in fig. 1. The upper panels show, for time $t = 800$, the mass per unit frequency ratio M_R of particles having a given value of the

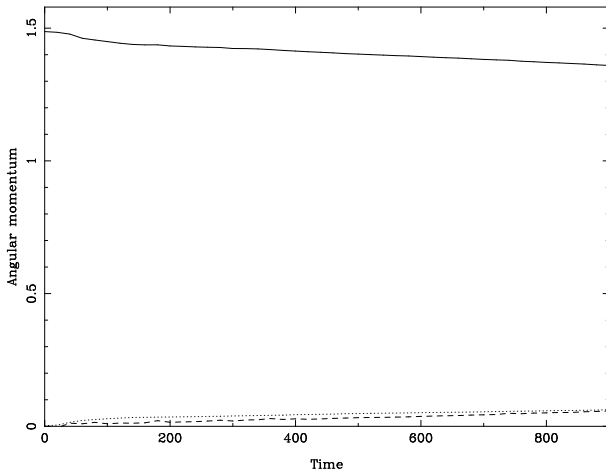


Figure 2. Angular momentum as a function of time for the disc component (solid line), the halo (dashed) and the bulge (dotted) of model MB0.

frequency ratio $(\Omega - \Omega_p)/\kappa$ as a function of this frequency ratio. As was already shown in A02, there are clear peaks, indicating the existence of resonances. The highest peak for the disc component is at the ILR, followed by $(-1, 6)$ and CR. In all simulations with strong bars the ILR peak is strong. The CR peak is also always present, but not always of the same amplitude. For MH-type cases, as the one shown in fig. 1, it is small, while in MD-types it is very important. The existence of peaks at other resonances, as well as their importance, varies from one run to another and also during the evolution of a given run. For the spheroidal component the highest peak is at CR, followed by peaks at the ILR and OLR. The peaks at the OLR are more important, both for the disc and the spheroid, for MD-type simulations.

The lower panels show the angular momentum exchanged. For this I calculated the angular momentum of each particle at time 800 and time 500, as described in section 4, and plotted the difference as a function of the frequency ratio of the particle at time 800. It is clear from the figure that disc particles at ILR lose angular momentum, while those at CR gain it. The $(-1, 6)$ also loses angular momentum. There is also a general, albeit small, loss of angular momentum from particles with frequencies between CR and ILR. This seems more important for simulations with haloes with smaller cores, as e.g. M γ 1 and M γ 2. It could be partly due to particles trapped around secondary resonances, and partly due to angular momentum taken from particles which are neither resonant, nor near-resonant, but can still lose a small amount of angular momentum because the bar is growing, as was discussed in section 2. The corresponding panel for the spheroid is, as expected, more noisy, but shows that particles at all resonances gain angular momentum. The gain at the OLR is more prominent for MD-type simulations, both for the disc and the spheroid component. To summarise we can say that this plot, and similar ones which I did for other simulations, confirm the results of section 2 and show that the linear results concerning the angular momentum gain or loss by resonant particles, qualitatively at least, carry over to the strongly nonlinear regime.

The evolution of the total angular momentum of the three components, disc, halo and bulge, for simulation MB0 is given in fig. 2. It shows what one would expect after having seen fig. 1, namely that the angular momentum of the halo and bulge components increases steadily with time, while that of the disc decreases. I made such plots for all my simulations and found qualitatively similar results. However, the amount of angular momentum exchanged varied widely from one simulation to another, varying from just a few percent, to near 35 percent. Linear theory predicts that the angular momentum exchanged would be highest if the disc and spheroid components have high density and low velocity dispersion, at least in the regions of the resonances. In such cases the bars should be strong and their pattern speed would decrease strongly with time. Thus the wide possible range of exchanged angular momentum should be followed by a wide range of possible bar strengths and possible pattern speed decreases. I will address this prediction in the following sections.

6 VELOCITY DISPERSION IN THE DISC COMPONENT

The disc mass and scale length are used here as units of mass and length. Therefore the only disc property that I can alter in order to influence the angular momentum exchange is its velocity dispersion. The linear theory given in section 2 predicts that for a given bar strength, the amount of angular momentum that can be emitted or absorbed at a disc resonance, depends on the velocity dispersion of the disc material. Thus a cold disc should emit/absorb considerably more at a given resonance than a hot one. Furthermore, from eq. (9) one can see that this should influence the pattern speed of the bar.

I made two different types of simulations in order to assess these effects. In the first class of simulations I used initial conditions where Q_{init} is constant with radius (as in AM02), and compared the results for different values of Q_{init} . Preliminary results of these simulations can be found in Athanassoula (2002b), and I will discuss them further here.

I ran a sequence of 8 simulations, with $M_d = 1$, $M_h = 5$, $R_d = 1$, $z_0 = 0.2$, $\gamma = 0.5$ and $r_c = 10$. They differ by their Q_{init} value, which was for the coldest 0.1 and for the hottest 2.2 and are listed in Table 1 as MQ1 to MQ8. This sequence of simulations shows clearly that the decrease of the bar pattern speed with time is a function of the velocity dispersion of the disc particles, in the sense that in colder discs the bar pattern speed decreases much faster than in hotter discs. In the limit of a sufficiently high Q_{init} , there is hardly any decrease. This is illustrated in Fig. 3, where I plot the pattern speed as a function of time for the five hottest simulations in the sequence, with Q_{init} ranging between 1.4 and 2.2. During the initial stages of the evolution the bar is not well developed, so its pattern speed is not well determined. One should thus not heed the initial abrupt decrease. After the bar has fully developed the pattern speed shows a very strong decline with time for the coldest case and hardly any decline for the hottest one. All 8 simulations are compared in Fig. 4, where I plot the slowdown of the bar between times 500 and 600 as a function of Q_{init} . It

confirms the trend seen in Fig. 3, showing a definite dependence of the slowdown rate on Q_{init} . The coldest simulation, for $Q_{init} = 0.1$, has well over four times the slowdown rate of the hottest simulation, for $Q_{init} = 2.2$. For the latter the slowdown rate is indeed very small, less than 0.005, i.e. of the order of three percent in $\Delta t = 100$, or, using the calibration proposed in section 4, in 1.4 Gyrs. In Fig. 4 I have also added the least squares fit to the data, which is only meant to guide the eye.

I have also made two simulations for which Q_{init} decreases exponentially with radius (Hernquist 1993). An MH-type such simulation is listed in Table 1 as simulation MQV1. I have taken $Q_{init}(r = 0.1) = 0.9$, so that a comparison between MQV1 and MQ2 can show the effects of a hotter outer disc region. The results of the two simulations differ only little. The difference between the relative Fourier components is less than 10 per cent of the maximum and is, after the bar has fully grown, always in the sense that run MQ2 has the strongest bar. The difference between the pattern speeds is of the same order, or smaller, in the sense that for MQV1 the pattern speed decreases less fast than MQ2. All this is in good agreement with the picture of bar evolution presented here. Indeed in run MQ2 most of the absorbing material is in the halo and only a small fraction is in the disc. Thus, making this small fraction less efficient, by heating the corresponding part of the disc, does not have much influence. In the inner disc part, where the emitters are situated, the difference in the initial Q is not large. Thus the results of the two runs do not differ much. The small difference between the two runs is also in the sense that could have been predicted by the picture of bar evolution presented here. Indeed MQ2 has the somewhat stronger bar, whose pattern decreases somewhat faster, which could be predicted since the outer parts of the disc are hotter.

An MD-type simulation with a variable Q_{init} is listed in Table 1 as MQV2. In this case $Q_{init}(r = 0.1) = 1$, so that a comparison between MQV2 and MDQ can show the effects of a hotter outer disc in MD-type simulations. This is much larger than in the case of MH-types. Indeed the $m = 2$ Fourier component drops by 30 to 40 percent, while the difference in the slowdown rate is considerably larger. Again this is in good agreement with the picture of bar evolution presented here. In MD-types the outer parts of the disc should contribute significantly to the angular momentum absorption. Thus making them hotter should lead to a considerably weaker bar whose pattern speed decreases considerably less. This is indeed borne out by the comparison of MQV2 and MDQ.

7 HALO-TO-DISC MASS RATIO

The analysis in section 2 shows that, all other parameters being the same, the amount of angular momentum that can be emitted/absorbed at a given resonance is proportional to the amount of mass at this resonance. In this section I will test this with the help of N -body simulations with haloes of different mass, or of different mass distribution.

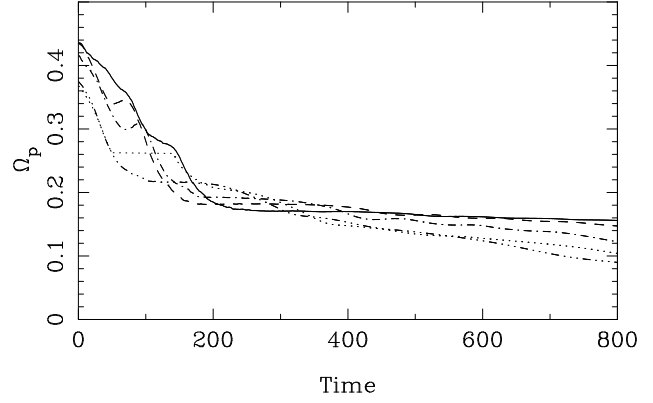


Figure 3. Bar pattern speed as a function of time, for simulations MQ4 ($Q_{init} = 1.4$, dot-dot-dot-dashed), MQ5 (1.6, dotted), MQ6 (1.8, dot-dashed), MQ7 (2, dashed) and MQ8 (2.2, solid line).

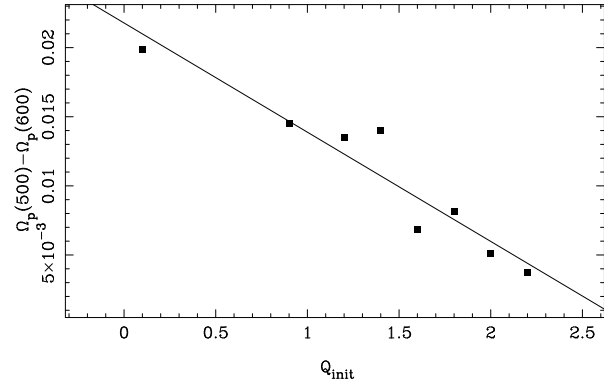


Figure 4. Slowdown of the bar between times 500 and 600 as a function of Q_{init} for simulations MQ1 to MQ8.

7.1 Halo density

Some insight can be gained already by comparing MH-type and MD-type models. Such comparisons, for various initial condition parameters, can be found in AM02, A02, or Athanassoula (2002b). These papers show clearly that stronger bars can grow in more halo dominated models, so I do not include further figures here. Figures 5 and 6 show the slowdown of the bar pattern speed as a function of the halo core size γ for a sequence of six models listed in Table 1 as M γ 2 to M γ 7. As already mentioned, MH-type haloes correspond to low values of γ and MD-types to high values. As predicted, MH-type models have pattern speeds that decrease faster than those of MD-types and there is a definite trend between the slowdown rate and γ . This is in agreement with the results of Debattista & Sellwood (1998, 2000), who find a strong temporal decrease of the pattern speed for halo dominated cases and a weak one for disc dominated cases. Figure 7 plots $F_{m=2}$, the maximum of the $m = 2$ relative Fourier amplitude, as a function of the core radius γ . It shows a clear trend in the sense that the bars formed in more concentrated haloes – i.e. in MH-types – are considerably stronger than those in less concentrated haloes –

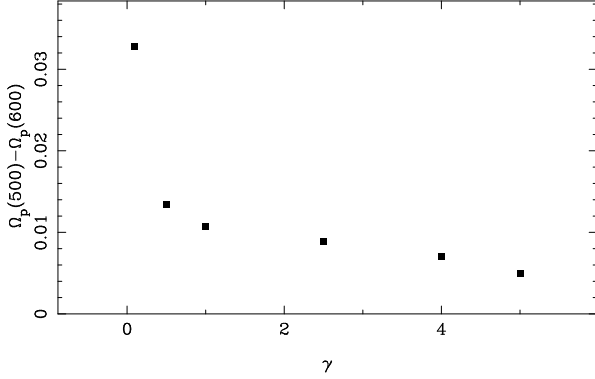


Figure 5. Slowdown of the bar pattern speed between times 500 and 600 as a function of the halo central concentration for simulations M γ 1, M γ 2, M γ 3, M γ 4, M γ 5, M γ 6 and M γ 7.

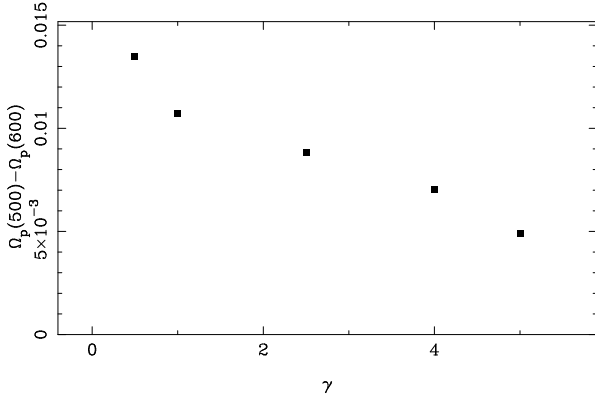


Figure 6. Blow-up of the lower part of the previous figure, showing that the trend with central concentration is clear even for higher values of γ .

i.e. in MD-types –. The trend is reversed in the innermost parts. The angular momentum gained by the halo also varies considerably along this sequence of runs. In fact more angular momentum is exchanged in simulations with lower γ , and that up to and including $\gamma = 0.5$. For this γ value the angular momentum gained by the halo is about 2.6 times higher than for $\gamma = 5$. For the smallest value of γ the angular momentum is slightly smaller than for $\gamma = 0.5$, i.e. show a similar behaviour to that of the $F_{m=2}$. Thus this sequence of simulations shows clearly that the strongest bars are associated with cases with more angular momentum exchange.

In order to understand better the effect of the halo on the evolution I will now consider haloes with masses which are lower than those in the simulations discussed so far. For this I will use a sequence of three simulations, all with $\gamma = 0.5$ and different values of M_h . They are listed in Table 1 as simulations M γ 3, MH1 and MH2. Some of their basic results are summarised in Fig. 8. In the initial stages of the simulation the bar grows slower in the more halo dominated environment, as expected (e.g. Athanassoula & Sellwood 1986). Nevertheless, the situation is eventually reversed, so that

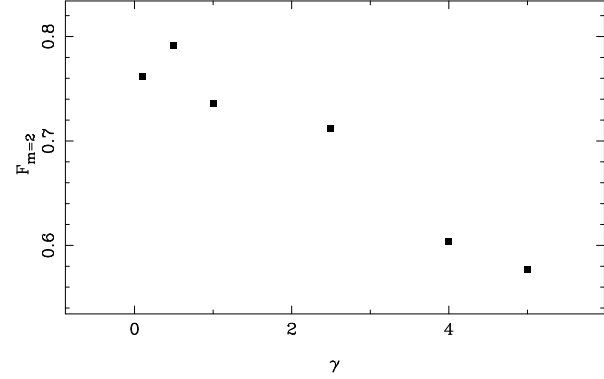


Figure 7. Maximum of the relative $m = 2$ Fourier component, $F_{m=2}$, at time 800 as a function of the initial halo central concentration for simulations M γ 1, M γ 2, M γ 3, M γ 4, M γ 5, M γ 6 and M γ 7.

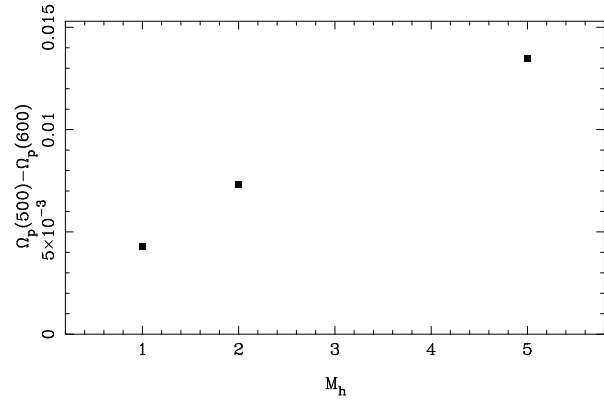


Figure 9. Slowdown of the bar pattern speed between times 500 and 600 as a function of the halo mass for simulations M γ 3, MH1 and MH2.

at later times the simulation with the most massive halo has the strongest bar. The other two simulations, with considerably less massive haloes, have also less strong bars. In particular, model MH2, which has the less massive halo, has also the weakest bar, and its $m = 6$ and 8 Fourier components do not stand out clearly from the noise, as was the case for model MD in AM02. The results of the three simulations differ also when seen side-on (i.e. with the line of sight along the bar minor axis), and a bulge-like protuberance out of the equatorial plane when seen end-on (i.e. with the line of sight along the bar major axis). As explained in AM02, this is just the bar seen end-on, and not a real bulge. Models MH1 and MH2 viewed side-on display a considerably less strong peanut, nearer to a boxy shape. This sequence, the one shown in Fig. 12 and other similar ones not shown here, reinforce the result found by AM02, namely that it is the strongest bars that form the strongest peanuts, or even ‘X’-shapes, while milder bars form boxy shapes. This is in agreement with observations (Lütticke et al. 2000), although of course the strength of the bar in edge-on galaxies can only

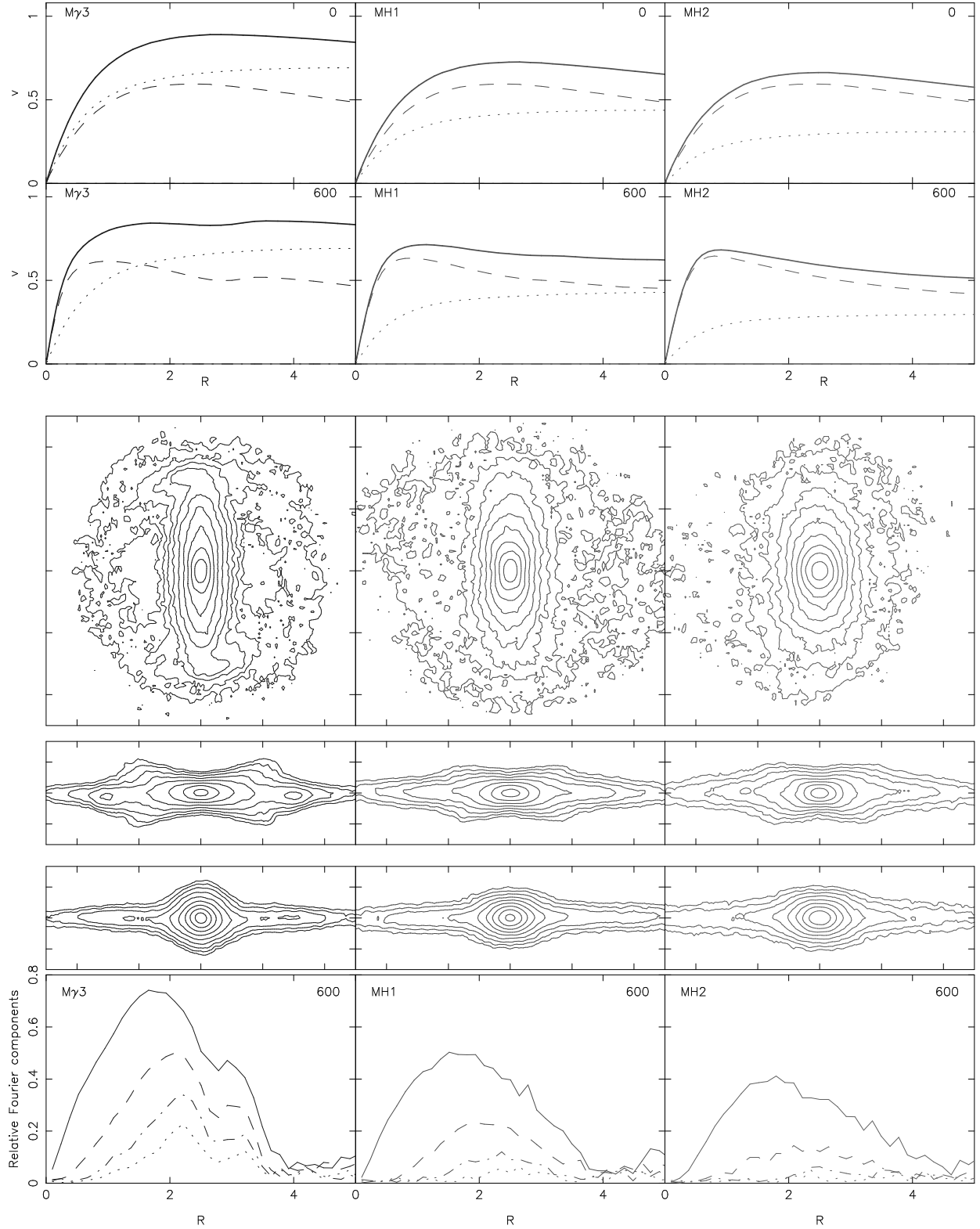


Figure 8. Basic information on three simulations with different disc masses, for time $t = 600$. Left panels correspond to simulation Mγ3, middle ones to simulation MH1 and right ones to simulation MH2. The two upper rows give the circular velocity curves at time 0 and 600. The dashed and dotted lines give the contributions of the disc and halo respectively, while the thick full lines give the total circular velocity curves. The third row of panels gives the isocontours of the density of the disc particles projected face-on and the fourth and fifth row give the side-on and end-on edge-on views, respectively. The side of the box for the face-on views is 10 length units and the height of the box for the edge-on views is 3.33. The isodensities in the third row of panels have been chosen so as to show best the features in the bar and in the inner disc. No isodensities for the outer disc have been included, although the disc extends well beyond the area shown in the figure. The sixth row of panels gives the $m = 2, 4, 6$, and 8 Fourier components of the mass, as defined in AM02.

be measured indirectly from the density drops on cuts along the equatorial plane.

The decrease of the pattern speed with time is shown for these three models in Fig. 9. There is a clear trend between the decrease of pattern speed and the halo mass, in the sense that the heaviest halo mass has the fastest decreasing pattern speed. The angular momentum gained by the halo also increases with the halo mass. Thus the halo of model M73 gains somewhat more than twice the angular momentum gained by the halo of model MH1, which in turn gains somewhat more than twice that gained by MH2. A plot similar to that of Fig. 1 shows that the height of the halo resonant peaks decreases drastically as M_h decreases. Thus this series of simulations confirms beautifully the predictions of the bar evolution picture presented here.

A similar sequence of simulations, now for $\gamma = 5$ (not listed in Table 1), shows different results (not plotted here). Indeed now the strength of the bar depends little on M_h , even though I have considered M_h values ranging from 1 to 5. The reason is that in MD cases, contrary to MH ones, the outer disc has a considerable contributions to the angular momentum absorption and is still capable of stepping in and providing the necessary sinks of angular momentum when the halo contribution is low.

The above should not give the false impression that by considering yet more massive haloes we will always get yet stronger bars, whose pattern speed will decrease yet faster. There is a limit beyond which the disc self-gravity is so small that the bar can not grow. Furthermore, by increasing the halo mass we also increase its velocity dispersion, thus decreasing its responsiveness. This effect will be discussed in detail in section 8.

To check the above I ran a series of six simulations with M_h between 5 and 10. Three are listed in Table 1 as MQ2, MH3 and MH4. The initial growth rate of the bar is lower in simulations with a higher halo mass, in good agreement with previous results (e.g. Athanassoula & Sellwood 1986). For $M_d/M_h = 0.2$ the bar is very strong, while for $M_d/M_h = 0.16$ both its strength and length are considerably smaller. In fact the difference is rather strong, for a decrease of the disc-to-halo mass ratio of only 20 per cent. A further 20 percent decrease results in a density distribution which has only a mild non-axisymmetry in the central parts, visible in the projected isodensities and in the $m = 2$ Fourier component.

Fig. 10 shows the bar pattern speed as a function of time, for two of the simulations discussed above. In simulation MQ2, which has a substantial disc component, the pattern speed drops considerably with time. On the other hand, the pattern speed hardly decreases in simulation MH3, whose disc-to-halo mass ratio is only 20 per cent less massive. The amount of angular momentum gained by the halo by time 900 is in MH3 5.7 times less than in MQ2. The difference is even more extreme for simulation MH4, whose halo gains only three percent of what was gained by the halo of MQ2. Thus this series of simulations confirms the prediction that less angular momentum exchange within the galaxy results in a weaker bar, whose pattern speed decreases less fast.

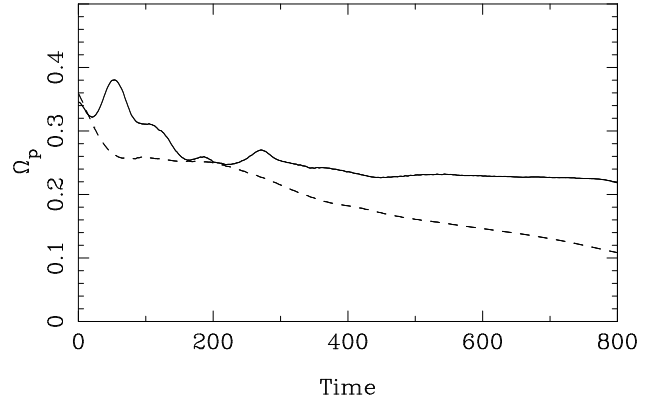


Figure 10. Bar pattern speed as a function of time, for two simulations with different disc-to-halo mass ratio. Simulation MQ2 (dashed line) has a $M_d/M_h = 0.2$, while simulation MH3 (solid line) has $M_d/M_h = 0.16$.

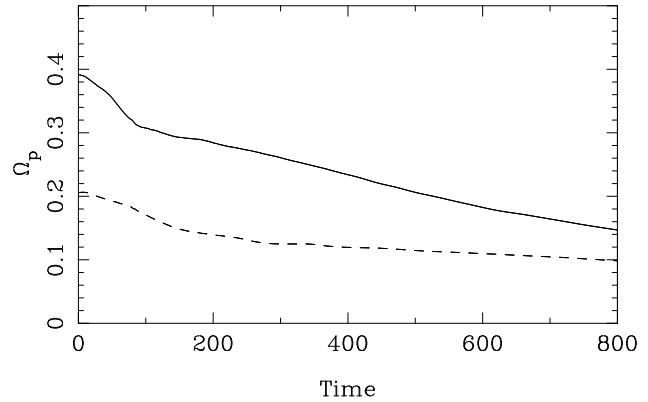


Figure 11. Bar pattern speed as a function of time, for a simulation with a bulge (MDB, solid line) and a simulation without (M77, dashed line).

7.2 Bulge component

I also ran 13 simulations including a bulge component with a mass between 0.2 and 0.6 and a scale length between 0.2 and 0.6. For MD type simulations the effect of the bulge is quite pronounced, in the sense that the strongest bars and peanuts form in models with the heaviest bulges. One example of such a case can be seen in Figures 1 and 2 of AM02, where one can compare the bar/peanut formed in simulations with and without bulge (models MD and MDB of that paper). The effect of the bulge is not as noticeable in MH type simulations.

The presence of the bulge also influences the slowdown rate of the bar, in the sense that the pattern speed of bars decreases much faster in the presence of a bulge than without it. The effect, as can be seen from Fig. 11, can be quite strong.

The effect of bulges, described above, is easily understood in the framework of evolution via angular momentum exchange by resonant stars. I have analysed the frequency of the orbits in the spheroids (i.e. bulge and halo together), as

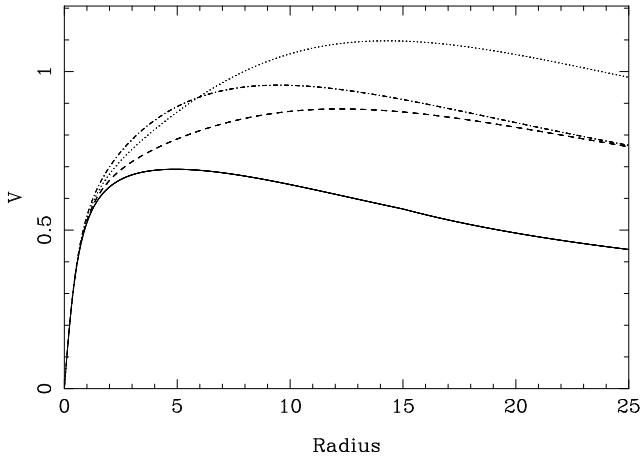


Figure 13. Rotation curve of the initial halo for model MQ2 (solid line), MHH1 (dashed line), MHH2 (dot-dashed line) and MHH3 (dotted line).

in A02, and found considerably more particles at resonance in cases with strong bulges. There is also, in general, more angular momentum exchange. This can explain why such models have stronger bars and faster slowdown rates.

Amongst the models I ran I have not encountered cases where a more massive bulge resulted in a less strong bar, as was the case for haloes, where, beyond a certain threshold, haloes hindered bar formation. This, however, could be due to the fact that I did not consider particularly massive bulges, or did not enhance their central concentration sufficiently.

8 VELOCITY DISPERSION OF THE HALO COMPONENT

One of the conclusions of section 2.2 is that, for a given bar strength, the amount of angular momentum that can be absorbed by a given halo resonance is larger if the distribution function is colder. Strictly speaking, this was shown only for haloes whose distribution function depends on the energy only. It should, however, be possible to extend this conclusion to a much wider class of reasonable distribution functions. In this case, and provided the halo is the main receptacle for the bar angular momentum, colder haloes should draw more angular momentum from the bars they harbour, than hot haloes. Since the bar is limited to the region within corotation, it is a negative angular momentum “perturbation”, and therefore will grow stronger in cases where more angular momentum will be taken from it, as I already discussed in section 2. I thus come to the conclusion that colder haloes should harbour stronger bars with faster decreasing pattern speed. I will now test these analytical predictions with numerical simulations.

The simplest way of increasing or decreasing the velocity dispersion in the halo component is to stay within the framework described in section 4, i.e. that of a spherical and isotropic halo, and increase or decrease the mass of the halo in its outer parts. Indeed in that case the halo radial velocity dispersion can be calculated from the collisionless Boltzmann equation as

$$\langle u_r^2 \rangle = \frac{1}{\rho_h(r)} \int_r^\infty \rho_h \frac{GM(r')}{r'^2} dr', \quad (27)$$

where $M(r)$ is the cumulative mass distribution. It is easy to see from the above equation that, for the same or similar ρ_h , mass distributions which extend to large radii will give larger values of $\langle u_r^2 \rangle$, i.e. hotter haloes.

Let me now compare the results of four simulations, MQ2, MHH1, MHH2 and MHH3. As given in Table 1, all four have identical disc mass distributions and Q values. The halo rotation curves of three of these simulations at the initial times are given in the upper panels of Fig. 12 for the inner region ($r < 5$ disc scale lengths) and for all four in the left panel of Fig. 13 for distances up to 25 disc scale lengths. The upper panels of Fig. 12 also give the disc and the total rotation curves. Within the inner 10 disc scale lengths the total rotation curve is flat, or, for MHH2, slightly rising, in all cases compatible with observed rotation curves.

Fig. 12 compares the basic morphological properties of the bar for three of the simulations, namely MQ2, MHH1 and MHH2. The most striking difference is between the lengths and strengths of the three bars. The former is clearly seen from the third row of panels, which shows the isophotes of the disc component. In the leftmost panel the bar length is of the order of 3 to 3.6[†] initial disc scale lengths, while in the rightmost one it is of the order of 1.5. I have given the above estimates in terms of the *initial* disc scale length, so as to permit direct comparison between the different cases. Indeed the disc scale length increases with time (Valenzuela & Klypin 2002) and the rate of increase could well be different for the simulations under comparison. Edge-on views show that simulations MQ2 and MHH1 have a peanut or ‘X’-shaped profile when viewed edge-on with the bar seen side-on (i.e. with the line of sight along the bar minor axis). On the other hand simulation MHH2 does not have any such shape, showing, at the best, a mild boxiness in the inner parts. The lower panels show that the amplitude of all m Fourier components decreases with increasing halo velocity dispersion. Also the location of the maximum moves to smaller radii as the halo velocity dispersion increases, i.e. as the bar length decreases.

Fig. 14 compares the three pattern speeds. It is clear that, although the pattern speed is a fast decreasing function of time for simulation MQ2, it hardly decreases for simulation MHH2. This is due to the fact that the halo in MQ2 is cold and thus its resonances can absorb a fair amount of angular momentum. On the contrary in MHH2 the halo is hot and thus its resonances can not act as an angular momentum sink. This again shows the importance of angular momentum exchange for the bar slowdown rate. It is also interesting to note that MHH2 is an example of a simulation with a strong halo and a hardly decreasing pattern speed. Thus it argues against a link between relative halo content and bar slowdown, and, more generally, against using the latter to set constraints on the former.

The angular momentum exchange also follows the sequence predicted by the analytic theory. Thus the angular momentum absorbed by the halo of simulation MQ2 is 1.6

[†] for a summary of the various methods used in measuring the bar length and the uncertainties involved see section 8 of AM02.

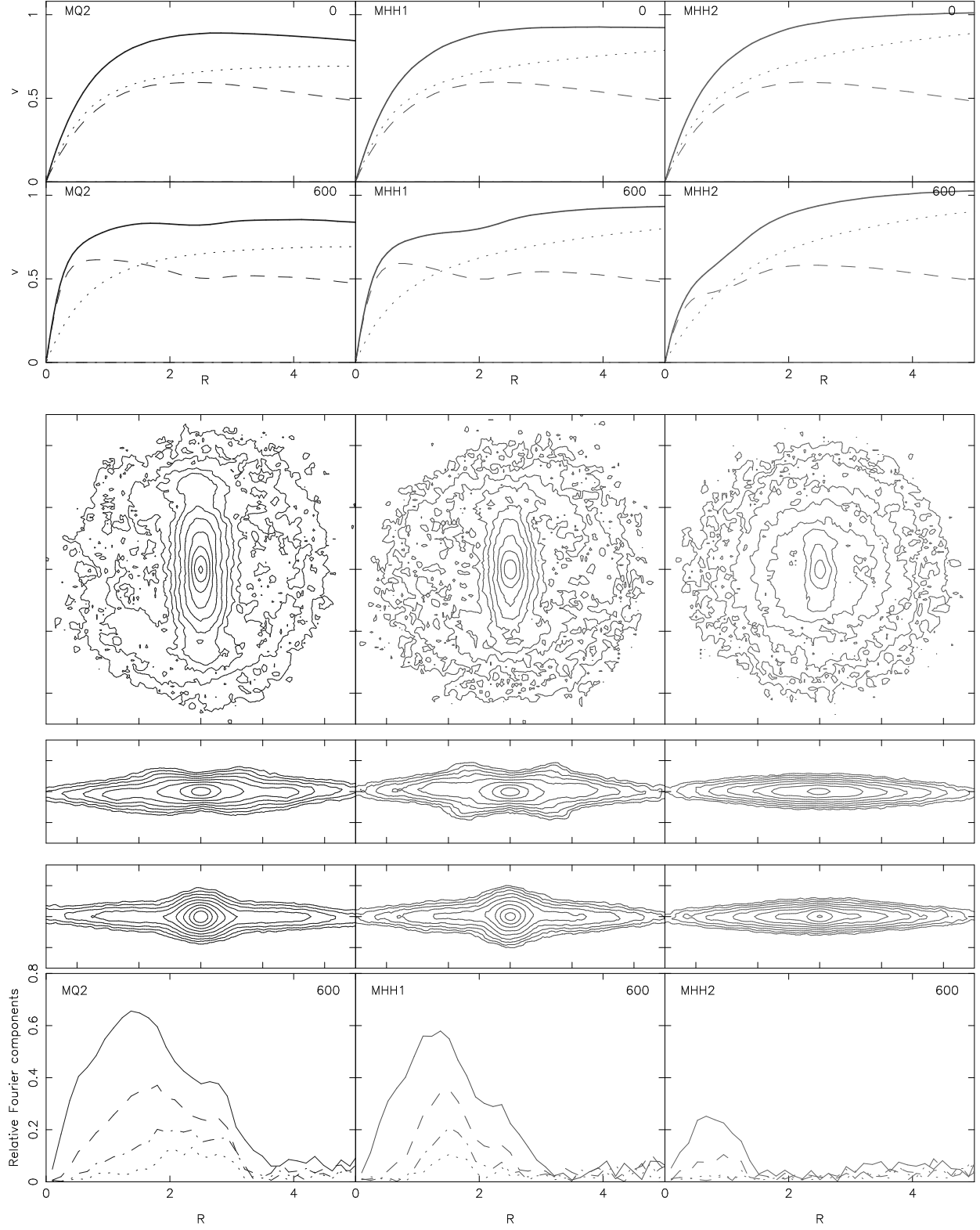


Figure 12. Basic information on three simulations with different halo components, at time $t = 600$. The layout is as for figure 8.

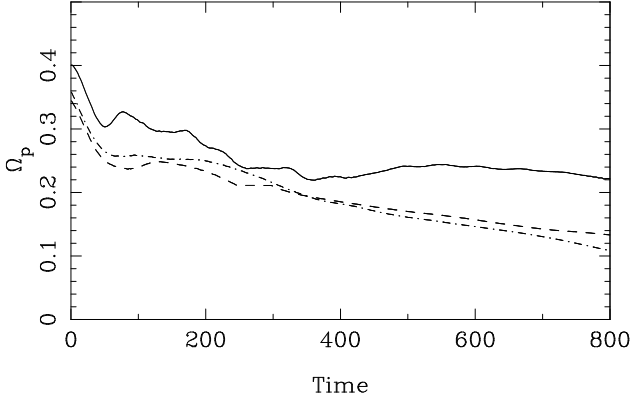


Figure 14. Bar pattern speed as a function of time, for simulations MQ2 (dot-dashed line), MHH1 (dashed line) and MHH2 (solid line).

times that for simulation MHH1, which in turn is 7 times that of MHH2. Thus this sequence of models behaves as expected by the analytical results and by the bar formation picture argued here.

9 CORRELATIONS

Eq. (8) predicts that the stronger the bar, the more the disc angular momentum will change. However, the angular momentum change does not only depend on the strength of the bar, but also on the distribution function at the resonant region. Similarly eq. (17) shows that the stronger the bar, the more angular momentum the halo will absorb. Again, however, the relation depends on the distribution function, this time of the halo component.

The relation between the angular momenta of the different components and the pattern speed is not as straightforward. The bar angular momentum is linked to the pattern speed via eq. (9), which includes the moment of inertia of the bar, which in turn depends on the bar strength and does not stay constant with time. Thus the relation of the angular momentum change to the pattern speed is more complicated than its relation to the bar strength.

Checking these relations with the bar angular momentum in the simulations is not straightforward, mainly because it is not straightforward to define the bar. One can of course attempt to define the outline of the bar, but several particles move in and out of it and thus are not easy to classify as belonging to the bar or not. The alternative approach is to define the bar as the total of the particles that are trapped around the x_1 , or x_1 -related orbits. Since these orbits, or their projections, close after one rotation and two radial oscillations, this is equivalent to defining the bar as the sum of the particles that are trapped around the $l = -1$ $m = 2$ resonance. This also, however, is not satisfactory, since bars contain particles that are trapped at other resonances, as well as chaotic orbits. I will thus avoid discussing the bar angular momentum and concentrate on the halo angular momentum. Since in the simulations presented here the halo is initially non-rotating, its total angular momentum at any time will be equal to the angular momentum it

has absorbed up to then. Similarly, since the disc starts as axisymmetric, the bar strength at any time represents also the global increase of the strength from the start.

I will start by following the change of the bar strength and pattern speed and the halo angular within a given run, and then compare ensembles of runs.

9.1 Individual simulations

The analytical work in section 2 predicts that, during the evolution, the bar will become stronger and its pattern speed will decrease, while the halo angular momentum will increase and that of the disc decrease. These effects have been qualitatively assessed in many simulations so far (e.g. Debattista & Sellwood 1998, 2000; Athanassoula 1996, 2002a,b, 2003). Here I will focus on the relations between these quantities during the evolution. Fig. 15 shows this in a quantitative way for two simulations with identical initial conditions, except for the parameter Q_{init} , which is constant with radius, but has a different value in the two cases. Both simulations have initially $M_d = 1$, $R_d = 1$, $z_0 = 0.2$, $M_h = 5$, $\gamma = 0.5$ and $r_c = 10$. Simulation MQ1 has $Q_{init} = 0.1$, i.e. starts off very cold, and simulation MQ2 has $Q_{init} = 2.2$, i.e. starts off very hot. They are extreme cases that show best the effect of Q_{init} , and have already been discussed in section 6. I have run a set of 8 simulations with intermediate values of Q_{init} and have found intermediate results. I will thus only describe the two extremes. Note that their evolution is quantitatively very different.

For the initially cold simulation both the pattern speed and the bar strength change in a similar way, so that their relation is simple and could, to a first approximation, be described by a single straight line in the (S_B, Ω_p) plane. This is not the case for the initially hot simulation, which has two distinct evolution phases. For this simulation the bar strength hardly increases during the first part of the evolution, while, during this time, the pattern speed decreases drastically[†]. Then, very abruptly, the situation changes and the pattern speed stops decreasing, while the strength of the bar starts increasing. The relation between the two quantities and the halo angular momentum is clear in the next two frames. Again for the initially cold disc the evolution is more gradual, while for the initially hotter one it is in two episodes.

9.2 Some global trends

Let me now turn to a more global view of the simulations. According to what has been said so far, I expect to find a trend between the strength and pattern speed of the bar and the angular momentum of the spheroidal component (i.e. halo plus bulge) of all models. These quantities are plotted in Figs. 16 and 17, while the corresponding correlation coefficients are given in Table 2. These are only given as indicative, and should not be taken too strictly. Indeed, the initial conditions of the various simulation were not taken so as to cover uniformly the available parameter space. Rather, they were made so as to follow interesting results, and these

[†] Note that during this stage the pattern speed is poorly defined.

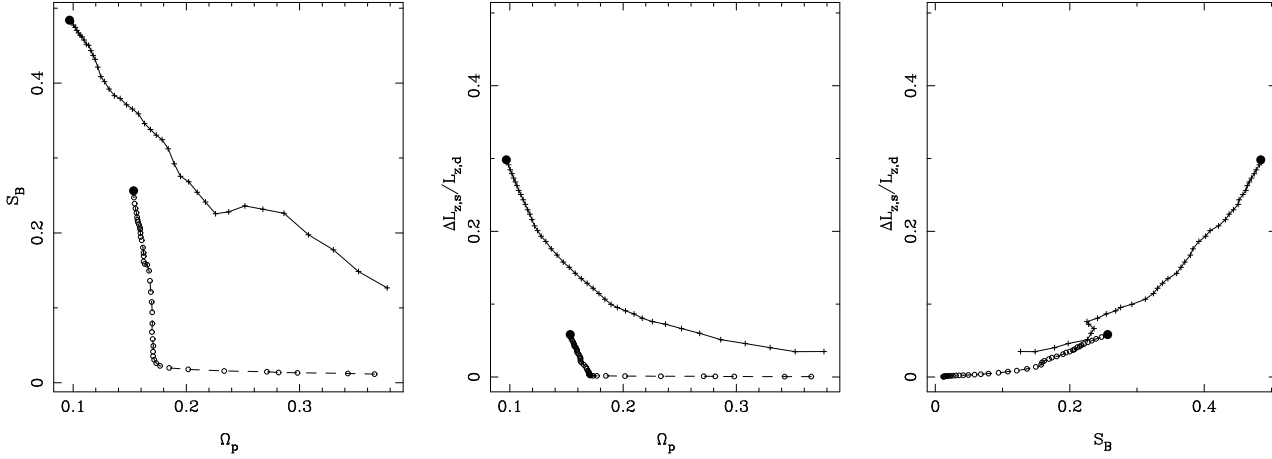


Figure 15. Relations between the bar strength and the pattern speed (left panel), the halo angular momentum and the pattern speed (middle panel) and the halo angular momentum and the bar strength (right panel). The halo angular momentum is normalised to the initial disc angular momentum ($L_{z,d}$). The times plotted start with time 60, to ensure that the bar has grown somewhat, so that the pattern speed can be measured, and go to the end of the simulations, at time 900. The last time is marked with a filled circle. The evolution for the simulation with the initially cold disc ($Q_{init} = 0.1$) is given with a full line and crosses. That of the initially hot disc ($Q_{init} = 2.2$) by a dashed line and open circles.

Table 2. Correlation coefficients

	(S_B, Ω_p)		$(\frac{\Delta L_{z,s}}{L_{z,d}}, \Omega_p)$		$(\frac{\Delta L_{z,s}}{L_{z,d}}, S_B)$	
	N_s	r_{cor}	N_s	r_{cor}	N_s	r_{cor}
All simulations	125	-0.83	116	-0.76	116	0.95
$.8 \leq Q_{init} \leq 1.2$	54	-0.88	51	-0.89	53	0.97
$Q_{init} < 0.3$	13	-0.88	13	-0.83	13	0.99
with bulge	13	-0.96	13	-0.90	13	0.95
$\gamma < 2$	49	-0.74	51	-0.89	48	0.84
$0.1 \leq \gamma \leq 0.5$	40	-0.79	41	-0.94	38	0.88
$\gamma = 0.01$	3	-0.87	-	-	-	-
$\gamma \geq 5$	46	-0.74	39	-0.55	39	0.91
$\gamma \geq 5$, cold	40	-0.63	33	-0.42	33	0.88
$\gamma \geq 5$, hot	6	-0.90	6	-0.74	6	0.94

may occur in restricted areas of the parameter space. Nevertheless, seen the large number of available simulations, the correlation coefficients should definitely give indications of trends and correlations. In each case, I list first the number of relevant simulations, N_s , and the the corresponding correlation coefficient.

The upper row in figures 16 and 17 includes all simulations available by the end of July 2002, except for some simulations which were run for test purposes, e.g. with a very low number of particles or a very large softening and a few for which some data were accidentally lost.

Eq. (17) leads us to expect a very tight relationship between the spheroidal angular momentum and the bar strength. This prediction is indeed borne out by the upper panel of Fig. 16. Table 2 gives for this relation a correlation coefficient of 0.95. This is a high value, particularly if one takes into account the fact that the plotted quantities (and particularly the bar strength) have measurement errors and

that eq. (17) includes e.g. the halo distribution function, which could differ from one case to another.

Section 2 predicts also trends for the bar pattern speed. The upper row in Fig. 16 confirms this expectation. There is an anti-correlation between the bar strength and pattern speed, albeit less tight than with the spheroid angular momentum, while the relation between the spheroid angular momentum and the pattern speed seems to have two distinct parts. These will be discussed further below.

The remaining panels of Figs. 16 and 17 use only subsamples of simulations. Indeed for such subsamples I expect to have more homogeneity of e.g. the distribution function which influences the relationships between the three quantities.

The middle row of panels concentrates on simulations which have Q_{init} around 1. I have here retained only simulations with $0.8 \leq Q_{init} \leq 1.2$. As can be seen from the figure and the corresponding coefficients in Table 2, the correlations and trends have, as expected, tightened considerably. The lower row of panels focuses on simulations with $Q_{init} < 0.3$, i.e. initially very cold. Now the correlation between the spheroid angular momentum and the bar strength has reached a correlation coefficient of 0.99.

The upper row of panels of Fig. 17 includes only simulations with bulges. They also form correlations, with the (S_B, Ω_p) and $(\Delta L_{z,s}/L_{z,d}, S_B)$ ones being rather strong (correlation coefficient of -0.96 and 0.95, respectively). A closer look shows that they do not cover exactly the same area as the simulations without bulges. This is particularly clear in the (S_B, Ω_p) case, where they lie above and to the right of the area covered by the remaining cases. This displacement is particularly strong for simulations with large bulges.

The middle row of panels includes only simulations with live haloes with $M_{h2} = 0$, $M_{h1} = 5$ and a small core radius ($\gamma < 2$) i.e. MH-type simulations. They present tight correlations, particularly those including the spheroid angular

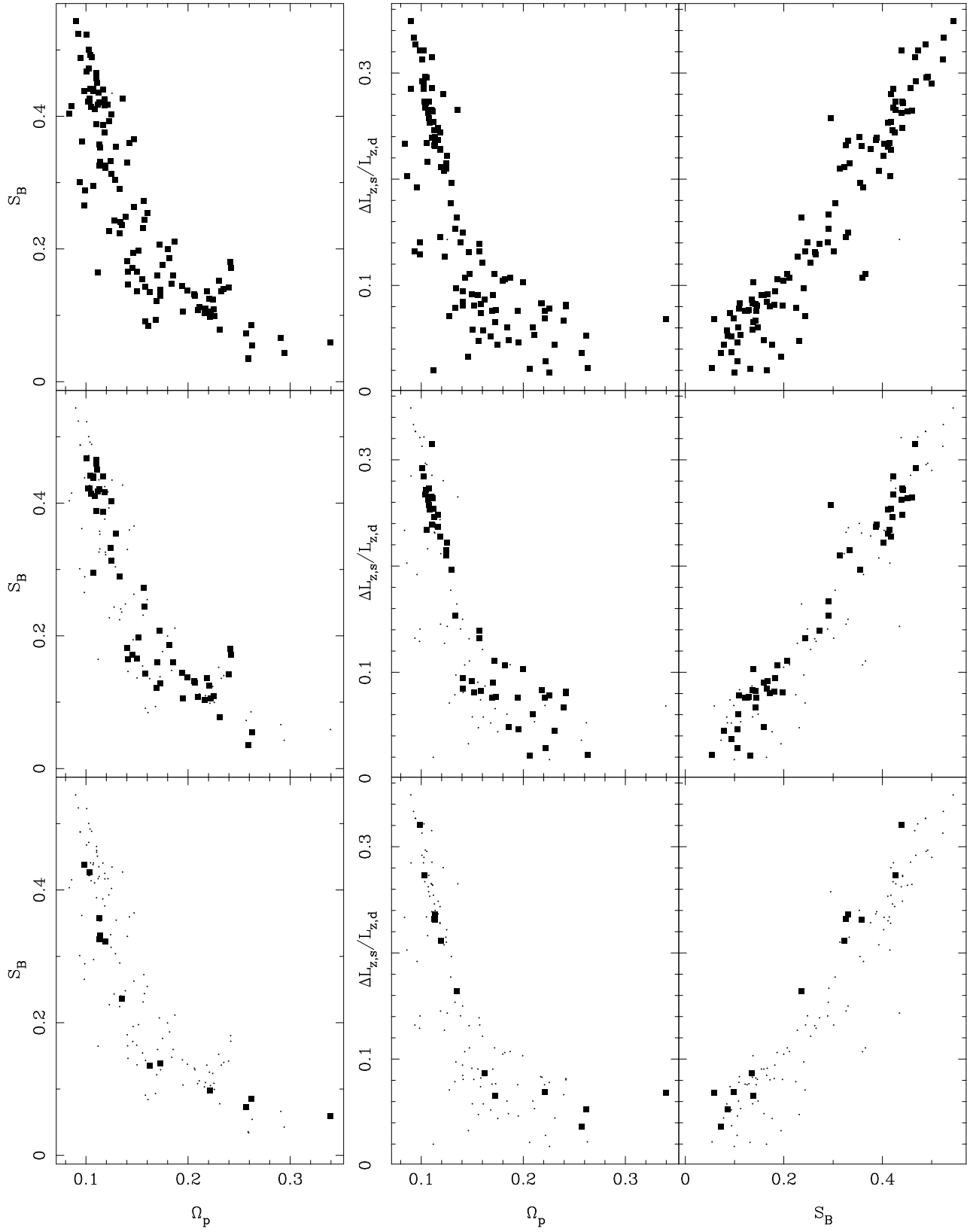


Figure 16. Relations between the bar strength and the pattern speed (left panels), the spheroid angular momentum and the pattern speed (middle panels) and the spheroid angular momentum and the bar strength (right panels), at times $t = 800$. The spheroid angular momentum is normalised by the initial disc angular momentum ($L_{z,d}$). The simulations under consideration in each panel are marked with a filled solid square and the rest by a dot. The upper row includes most simulations, the middle one those with $0.8 \leq Q_{init} \leq 1.2$ and the lower one those with $Q_{init} < 0.3$.

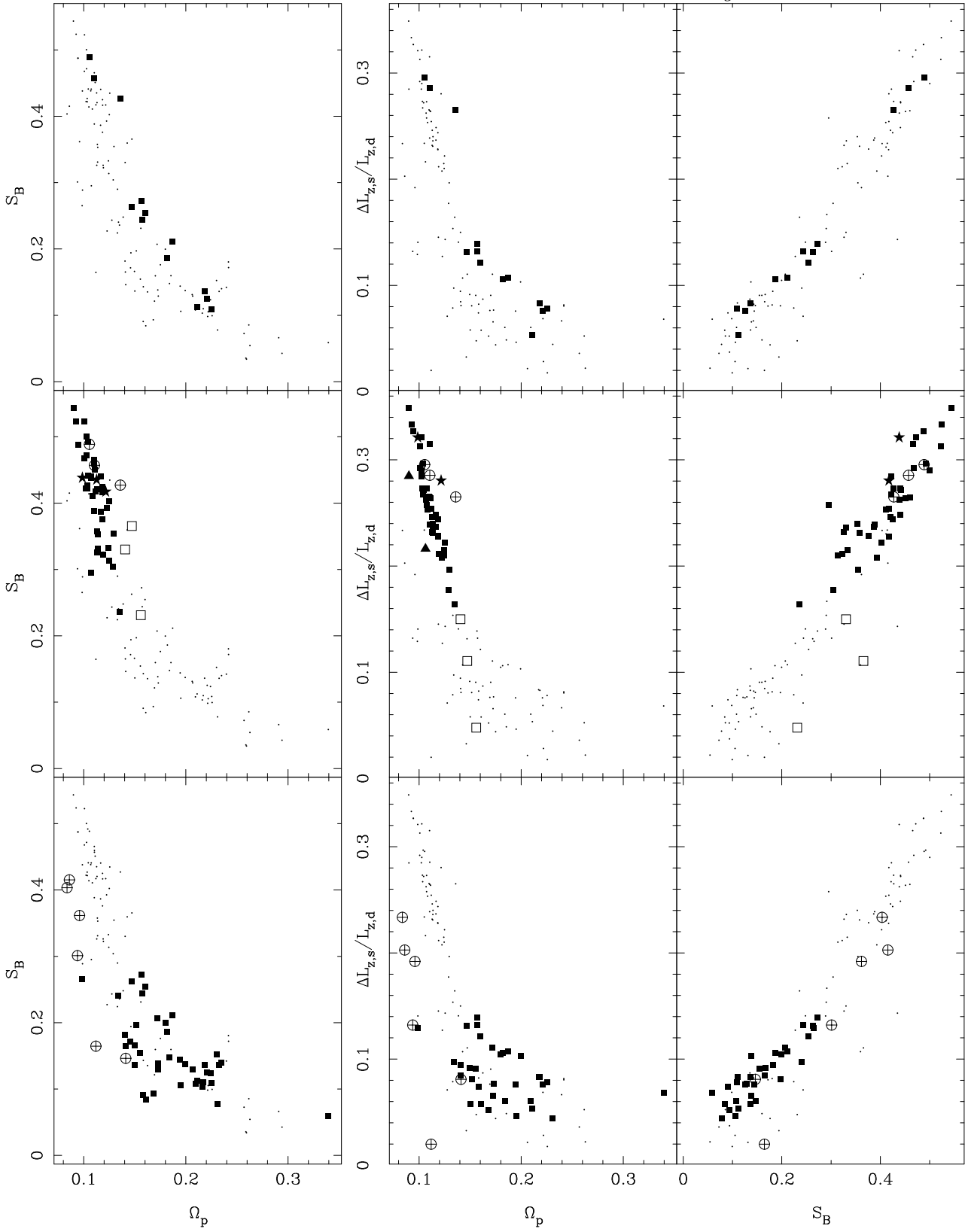


Figure 17. Same as the previous figure but for different cases. The upper row includes simulations with bulges, the middle one simulations with a halo with $M_{h2} = 0$, $M_{h1} = 5$ and $\gamma < 2$ and the lower one simulations with a halo with $M_{h2} = 0$, $M_{h1} = 5$ and $\gamma > 2$. In the middle panel simulations with a bulge are marked with a \oplus , simulations with $\gamma = 0.01$ with a filled star, simulations with $\gamma \geq 1$ with a filled triangle and simulations with $Q_{init} \geq 2$ with an open square. In the lower panel simulations with $Q_{init} \geq 1.4$ and $z_0 \geq 0.2$ are marked with an \oplus .

momentum. To examine this further I plot with different symbols simulations with $\gamma < 0.02$ (filled stars), simulations with $\gamma > 0.9$ (filled triangles) and simulations with bulges (crosses within an open circle). All the remaining simulations have $\gamma = 0.5$, except for one which has $\gamma = 0.1$. They show a very tight anti-correlation in the $(\Delta L_{z,s}/L_{z,d}, \Omega_p)$ plane (correlation coefficient of -0.94). This is predicted in the discussion following eq. (9), where a correlation is predicted between the spheroid angular momentum and the bar pattern speed, if the main receptacle of angular momentum is the halo. This should indeed be the case for MH-type simulations. Thus the tight anti-correlation found is yet another argument in favour of the bar evolution picture proposed here.

Finally the lower panels correspond to cases with $M_{h2} = 0$, $M_{h1} = 5$ and a large core radius ($\gamma \geq 5$), i.e. to MD-type cases. Their behaviour is totally different from that of the MH-type cases. The only correlation worth mentioning is the one between the spheroid angular momentum and the bar strength. The striking difference between the cases with a small core radius ($\gamma < 2$, middle panels) and those with a large core radius ($\gamma \geq 5$, lower panels) could be predicted from the framework presented here. Indeed in the cases with a small core radius the halo is the main recipient of angular momentum, as discussed above, and there should be correlations between the angular momentum it has acquired and the bar properties. On the other hand for cases with a large core radius, then the outer disc may also absorb a non-negligible part of the angular momentum, and thus a correlation with the halo angular momentum only would be less tight. This is better understood if we consider separately in the lower panels the cases with hot discs, i.e. $Q_{init} \geq 1.4$ and $z_0 \geq 0.2$ (crosses within an open circle), and the colder cases (filled squares). It is interesting to note that they form separate, clear sequences in all three planes, as could be expected from the scenario I propose here. Indeed if the outer disc is hot, then the spheroid should be the main angular momentum sink and thus trends or correlations with the spheroid angular momentum should be expected. On the other hand if the outer disc is cold, then both it and the spheroid should be sinks of angular momentum, and a trend or correlation with the angular momentum absorbed by only one of the two will not necessarily exist, or will be more loose. All this is well borne out by the relations in the lower panels.

10 SUMMARY AND DISCUSSION

In this paper I discussed the role of angular momentum exchange in determining the length, the strength and the slowdown rate of bars. In order for the bar to grow, it has to shed angular momentum, and, for that, there must be resonant material to receive it. Such material can be found either in the outer disc, or in the halo. It is this exchange that drives the bar evolution and determines its strength and length as well as its slowdown.

The galaxy strives to transfer angular momentum outwards (LBK), while keeping an equilibrium between emitters and absorbers. Emitting can be hampered by increasing the disc velocity dispersion within CR (section 6). There will then be only little angular momentum exchange – even if the halo has the possibility of absorbing considerable amounts

– and this will limit the pattern speed decrease and the bar strength. Absorbing by the outer disc can be hampered if that part of the disc has low density, or is hot (section 6). Absorbing by the spheroid is hampered if that component is hot, or rigid (section 8), or has relatively little mass in the resonant regions (section 7.1). More angular momentum exchange leads to stronger bars, whose pattern speed decreases faster. To make the role of the angular momentum exchange yet clearer I presented trends and correlations between the exchanged angular momentum and the bar strength and pattern speed.

As discussed in section 3, in order to shed angular momentum the bar can slow down, or become longer, or thinner. The N -body simulations have shown that it chooses to follow all three alternatives, but to a degree that varies from one simulation to another and also sometimes during different phases of the evolution. More work is needed to explain this behaviour.

If the galaxy is isolated, there should be as much angular momentum emitted as there is absorbed, i.e. there should be an equilibrium between emitters and absorbers. This equilibrium influences the evolution of the pattern speed. Indeed, if the pattern speed is lowered, corotation will move outwards and there will be more emitters and less disc absorbers. Thus in galaxies in which the halo can not absorb much angular momentum, either because of its low density or because of its high velocity dispersion, corotation should be at a relatively small radius to make space for sufficient absorbers in the disc component. On the other hand, in galaxies with a strong and responding halo component, corotation can be at larger radii. This will maximize the number of emitters, while the absorption will be assured mainly by the halo. These predictions are indeed borne out by the simulations presented here. Indeed MH-type simulations have longer bars than MD-types. Also the pattern speed of MH-type bars decreases faster than that of MD-types.

The considerations in this paper argue that it is very hazardous to set limits to the relative halo mass from the bar slowdown rate. I have shown here that this slowdown depends not only on the relative halo mass, but also on the velocity dispersion of both the disc and the halo (bulge) component. Indeed, in sections 6, 7, and 8 I gave examples showing the crucial importance of these parameters. Models MH3 and MHH2 have a very strong halo. Yet their pattern speed hardly decreases. A similar comment can be made for model MQ8. Furthermore, the reason for this is not the same in all cases. In model MHH2 the halo is too hot to be able to absorb, while in model MQ8 the disc is very hot, thus hampering both emitters and disc absorbers. In all these cases the pattern speed decrease is of the order of, or less than, 0.005 in a Δt of 100 computer units. Applying the calibration proposed in AM02, I find that this corresponds to a decrease of the pattern speed of the order of, or less than, 0.35 km/sec/kpc in 1.4 Gyrs. This decrease is considerably less than the observational errors when measuring the pattern speed (see e.g. Gerssen 2002 for a compilation). It thus can not be excluded that disc galaxies have a high halo-to-disc mass ratio and at the same time a hardly decreasing pattern speed. Let me continue this argument further and assume that all bars were in place at about $z = 0.5$, i.e. 2 to 3 Gyrs ago. Then, for galaxies resembling simulations MHH2 or MQ8, the bar pattern speed would have decreased

by less than 1 km/sec/kpc since that time, again considerably less than observational errors, while their halo would be relatively very massive. One should thus not use the pattern speed slowdown as a way of setting a limit to the halo-to-disc mass ratio. Several other ways have been put forward for the case of barred galaxies (Athanasoula 2002b) and they will be discussed in some detail in a future paper.

Although the picture is now sufficiently clear for N -body bars, it is not straightforward to apply it to real galaxies. Of course, the trends I have found here should carry over. In other words, both the outer disc and the halo should be able to absorb more angular momentum if the resonant regions are more densely populated and/or if the resonant material is colder. Our knowledge, however, of the halo properties is rather limited, and does not allow us to go much further. The halo material could be elementary particles, or baryonic material of sub-stellar masses, or small black holes. In these cases the mass of each ‘halo particle’ ranges from smaller to *very* much smaller than the mass of the individual particle used in the present simulations. It should be sufficiently small to ensure that galactic haloes have low graininess and are thus far from the noise-dominated regime. Hence there should be considerable halo material at or near resonance, able to absorb angular momentum. The angular momentum exchange should thus be particularly strong, much more so than in the present simulations, in the case of a halo made of elementary particles having a relatively cold distribution function. On the other hand, the sub-clumps which could well exist in the halo would lower the capacity of the halo to absorb angular momentum to a level more comparable to what is found in the present simulations.

The mass and the density distribution of the halo material in the regions of interest is not well known, as witnessed by the fact that the debate between the maximum disc and the sub-maximum disc proponents is still going strong (see e.g. Bosma 1999 and 2002, and references therein). Even less is known about the axial ratio of the halo, about whether it has figure rotation, about its extent, and about how much, if at all, the material in it rotates. Finally, it is impossible to say anything about even basic properties of the halo distribution function.

Seen our very restricted knowledge about the halo properties, it might be useful to face the question from the opposite direction, i.e. to see what, if anything, these simulations can tell us about the halo. Unfortunately no strong conclusions can be obtained, although there are some suggestions and indications. Namely galaxies with strong bars should have offered a sufficient sink of angular momentum so that the bar could grow to its present strength. On the other hand weak bars must be in surroundings where the angular momentum exchange was limited. This could be either by a very extended, or otherwise hot, halo, or then a halo whose resonance regions are of low density.

The results presented in this paper explain well the observations discussed in the introduction. Thus bars can come in a broad range of strengths because the amount of angular momentum exchanged in their respective galaxies varies considerably from one case to another. In galaxies with weak, small bars – as e.g. our own Galaxy – little angular momentum should have been exchanged. The contrary should be true for galaxies with very strong bars. In this context it is worth mentioning that Gadotti and de Souza (2003a,

2003b) report on two galaxies with particularly strong bars. Most of the light in these two galaxies is in the bulge/bar component and very little in the disc. Making the reasonable assumption that the mass-to-light ratio of the two have similar values, I come to the conclusion that the bar has grown sufficiently in those galaxies to take over most of the material originally in the disc, and leave a very weak disc component. These galaxies would then be extreme cases of MH-type galaxies.

The correlation between bar lengths and bulge sizes, reported by Athanasoula & Martinet (1980) and by Martin (1995), can also be understood in this framework. Indeed the bulge is part of the spheroidal component and thus can help the bar grow by taking from it angular momentum. The more massive the bulge, the more angular momentum it can absorb and the longer the bar will grow. Finally, this framework explains why bars are stronger in early type galaxies than in later types. Indeed these galaxies are known to have stronger bulges, which will act as angular momentum sinks and thus simulate bar growth. Whether one can extend this argument further and deduce that early types should also have haloes which can act as a better sink of angular momentum than the haloes of late type galaxies, is not clear at this point. Detailed modelling of a few barred galaxies would be necessary to estimate how much angular momentum their bulges can take and thus to see to what extent the haloes of early type galaxies need to absorb more angular momentum than their counterparts in late types.

Rings are often observed in disc galaxies (e.g. Buta 1995, 1999) and their location is known to be linked to resonances (Athanasoula, Bosma, Crézé et al. 1982; Buta 1995, 1999). If the pattern speed decreases considerably with time the position of the rings will migrate outwards, while if the pattern speed hardly changes the ring position will also not change much. It would thus be interesting to pursue a detailed modelling, including also gas, star formation and stellar evolution, in order to see whether there could be observable signatures from ring migration on the population of the ring. It would then be possible to set constraints on the evolution of a disc galaxy from spectral observations of its ring(s).

Several simulations in the last few years have formed bars of very different length, strength and slowdown rate. These differences can now be easily understood in the framework presented here. Debattista & Sellwood (1998, 2000) reported results from relatively low resolution simulations (i.e. with a softening length equal to one fifth of the disc scale length and to twice the disc scale height), which start off very cold ($Q_{init} = 0.05$), while their haloes had a relatively short extent (12.6 disc scale lengths). My results here show that all their MH-type simulations should result in strong bars with sharply decreasing pattern speed, and indeed this is what their simulations gave. AM02, A02 and Athanasoula (2002a) presented simulations with a considerably smaller softening (in most cases 0.0625 of the disc scale length, or, equivalently, less than a third of the disc scale height; in some cases 0.03125), a wide range of Q_{init} and a somewhat more extended halo (15 disc scale lengths). These results are discussed in detail in this paper, and fit well the bar evolution picture presented here. Finally Valenzuela & Klypin (2002) have three simulations with Q_{init} higher than 1, and a very extended halo component (70 to 85

disc scale lengths). Their softening is variable and, at least in the innermost parts, very small. It is not clear at this stage whether the number of particles in the disc (200 000) and the inner halo is sufficiently large to prevent noise from influencing the evolution with this small a softening. The general evolution, however, is in good agreement with the picture presented here. Indeed, they report very little angular momentum exchange and bar slowdown rate, and their bars are somewhat shorter than those e.g. of AM02. This could be expected since their halo particles are too hot to absorb considerable angular momentum. Thus their results are to be compared with e.g. model MHH2 of the present paper.

The picture presented in this paper is rather complicated, since it includes various sinks (the material at resonance in the outer parts of the disc, as well as the halo resonant material) and is influenced by several properties of the galaxy. Even so, this picture is not complete and includes several major simplifications. One concerns the distribution function of the halo. Here I assumed a particularly simple case. However, since the form of the distribution function will influence the amount of angular momentum exchanged and therefore the strength and slowdown of the bar, it is interesting to examine other distribution functions to find what range of angular momentum exchanges can be covered. A second important point to consider is the existence of a gaseous component. This would be one more partner in the angular momentum exchange, complicating further the problem. Indeed, even if the gas mass is only a very small fraction of the total, it is very cold, considerably colder than both the disc and the halo. Thus its contribution to the angular momentum exchange process could well not be negligible.

A third effect is the shape of the halo. Although the flattening of the halo could influence the angular momentum exchange, in particular via the halo distribution function, I believe that the strongest effect would come from the possible non-axisymmetry of the halo. By this I do not mean the possible elongation of the halo in the inner region in response to the bar, which is anyway included in the simulations discussed here, since they are fully self-consistent. I mean the effect that a non-axisymmetry, present in the halo at large scale in the initial conditions, could have on the evolution in general. In such a case the halo and bar components could interact in a way reminiscent of mode-mode interaction often discussed in plasma physics, the one driving the other. Since cosmological simulations show the existence of strongly triaxial haloes, I will be addressing this very complicated problem in a future paper. A fourth related issue is the effect of companions, since galaxies are often not isolated, and thus a companion could be one more partner in the angular momentum exchange process. A first attempt at this problem is made by Berentzen et al. (2003).

A possible objection against the simulations presented here is that bars probably do not form in as quiet a way as that described here. Indeed here I assumed, as bar formation studies always do, that the disc is initially axisymmetric, with properties near to those of present day disc galaxies. In other words I assumed implicitly that the disc formed first and the bar later. This would be a reasonable hypothesis if bars are rare at high redshift, as argued by Abraham et al. (1999). If this is not the case and bars start growing

during the disc formation stage, then the detailed properties of the bar may be considerably different from those of the bars presented here. Nevertheless, this will not change any of the physics described here. Again it will be the angular momentum exchange that will influence the bar growth and slowdown, although the differences in the properties of the disc and halo from those assumed here may well change the *amount* of angular momentum exchanged, and thus the detailed bar properties. Since, however, I have studied here both qualitatively and quantitatively the effect of the disc and halo properties on the angular momentum exchanged, it should be possible, when the subject of disc formation history is more evolved, to apply the results found here to the proper disc formation scenario.

Acknowledgments. I thank M. Tagger, A. Bosma, W. Dehnen, C. Heller, I. Shlosman, F. Masset, J. Sellwood, O. Valenzuela, A. Klypin, P. Teuben and A. Misiriotis for many interesting discussions. I thank J. C. Lambert for his help with the GRAPE software and the administration of the simulations and W. Dehnen for making available to me his tree code and related programs. I also thank the INSU/CNRS, the University of Aix-Marseille I, the Region PACA and the IGRAP for funds to develop the GRAPE and Beowulf computing facilities used for the simulations discussed in this paper and for their analysis.

References.

- Abraham, R. G., Merrifield, M. R., Ellis, R. S., Tanvir, N. R. & Brinchmann, J. 1999, *MNRAS*, 308, 569
- Athanassoula, E. 1992, *MNRAS*, 259, 345
- Athanassoula, E. 1996, in “Barred Galaxies”, eds. R. Buta, D. Crocker and B. Elmegreen, *PASP conference series*, 91, 309
- Athanassoula, E. 2002a, *ApJ*, 569, L83 (A02)
- Athanassoula, E. 2002b, in “Galactic Discs : Kinematics, Dynamics and Perturbations”, eds. E. Athanassoula, A. Bosma and R. Mújica, *PASP conference series*, 275, 141
- Athanassoula, E. 2003, in “Galaxy Evolution: Theory and Observations”, eds. V. Avila-Reese, C. Firmani, C. Frenk and C. Allen, *RevMexAA*, in press
- Athanassoula, E., Bienaymé, O., Martinet, L. & Pfenniger, D. 1983, *A&A*, 127, 349
- Athanassoula E., Bosma, A., Crézé, M. & Schwarz, M. P. 1982, *A&A*, 107, 101
- Athanassoula, E. & Martinet, L. 1980, *A&A*, 87, L10
- Athanassoula, E. & Misiriotis, A. 2002, *MNRAS*, 330, 35 (AM02)
- Athanassoula E. & Sellwood J. A. 1986, *MNRAS*, 221, 213
- Berentzen, I., Athanassoula, E., Heller, C. H. & Fricke, K. J. 2003, in preparation
- Binney, J. & Tremaine, S. 1987, *Galactic Dynamics*, Princeton University press
- Bosma, A. 1999, *Celestial Mechanics & Dynamical Astronomy*, 72, 69
- Bosma, A. 2002, in “Galactic Discs : Kinematics, Dynamics and Perturbations”, eds. E. Athanassoula, A. Bosma and R. Mújica, *PASP conference series*, 275, 23

- Buta, R. 1995, *ApJS*, 96, 39
- Buta, R. 1999, *Ap&SS*, 269/270, 79
- Contopoulos G. 1980, *A&A*, 81, 198
- Contopoulos G., Grosbøl P. 1989, *A&AR* 1, 261
- Contopoulos G., Papayannopoulos, T. 1980, *A&A*, 92, 33
- Debattista, V. P., & Sellwood, J. A. 1998, *ApJ*, 493, L5
- Debattista, V. P., & Sellwood, J. A. 2000, *ApJ*, 543, 704
- Dehnen, W. 2000, *ApJ*, 536, L39
- Dehnen, W. 2002, *J. Comp. Phys.*, 179, 27
- Elmegreen, B.G., Elmegreen, D. M., 1985, *ApJ*, 288, 438
- Gadotti, D. A. & de Souza, R. E. 2003a, *ApJL*, 583, L75
- Gadotti, D. A. & de Souza, R. E. 2003b, in “The evolution of galaxies III From simple approaches to self-consistent models”, eds. G. Hensler, G. Stasinska, S. Harfst, P. Kroupa, Chr. Theis, Kluwer academic publishers, in press
- Gerssen, T. 2002, in “Galactic Discs : Kinematics, Dynamics and Perturbations”, eds. E. Athanassoula, A. Bosma and R. Mújica, *PASP conference series*, 275, 197
- Hernquist, L. 1993, *ApJS*, 86, 389
- Hernquist, L. & Weinberg, M. D. 1992, *ApJ*, 400, 80
- Kalnajs, A. J. 1971, *ApJ*, 166, 275
- Kato, S. 1971, *PASJ*, 23, 467
- Kawai, A., Fukushige, T., Makino, J., & Taiji, M. 2000, *PASJ*, 52, 659
- Kormendy, J. 1979, *ApJ*, 227, 714
- Little, B. & Carlberg, R. G. 1991a, *MNRAS*, 250, 161
- Little, B. & Carlberg, R. G. 1991b, *MNRAS*, 251, 227
- Lütticke, R., Dettmar, R.-J. & Pohlen, M. 2000, *A&A*, 362, 435
- Lynden-Bell, D. & Kalnajs, A. J. 1972, *MNRAS*, 157, 1, 1972 (LBK)
- Mark, J. W.-K. 1976, *ApJ*, 206, 418
- Martin, P. 1995, *AJ*, 109, 2428
- Ohta, K. 1996, in “Barred Galaxies”, eds. R. Buta, D. Crocker and B. Elmegreen, *PASP conference series*, 91, 37
- Reynaud D. & Downes D. 1997 *A&A*319, 737
- Sandage A. 1961, *The Hubble Atlas of Galaxies*, Carnegie Institution of Washington, Washington DC
- Sandage, A. & Bedke J. 1988, *Atlas of Galaxies*, NASA, Washington DC
- Sanders R. H., Tubbs A. D. 1980 *ApJ*, 235, 803
- Sellwood, J. A. 1980, *A&A*, 89, 296
- Skokos, H., Patsis, P. & Athanassoula, E. 2002, *MNRAS*, 333, 861, 2002
- Syget, J. F., Tagger, M., Athanassoula, E. & Pellat, R. 1988, *MNRAS*, 232, 733
- Tagger, M., Syget, J. F., Athanassoula, E. & Pellat, R. 1987, *ApJ*, 318, L43
- Tremaine, S. & Weinberg, M. D. 1984a, *MNRAS*, 209, 729
- Tremaine, S. & Weinberg, M. D. 1984b, *ApJ*, 282, L5
- Weinberg, M. D. 1985, *MNRAS*, 213, 451
- Valenzuela, O. & Klypin, A. 2002, *MNRAS*, submitted
- Van Albada, T. S. & Sanders, R. H. 1982, *MNRAS*, 201, 303